1 **A low cost, low power sap flux device for distributed and intensive monitoring of tree**
2 **transpiration**
3

4 Justin Beslity[1*], Stephen B. Shaw[1], John E. Drake[1], Jason Fridley[2], John C. Stella[1], Jordan

5 Stark[2], and Kanishka Singh[3]

6 [1] SUNY College of Environmental Science & Forestry Syracuse, NY, [2] Syracuse University Syracuse, NY, [3] Cornell University Ithaca NY
7 *Corresponding author. E-mail address: jobeslit@syr.edu (Justin Beslity).

8

9

10 **Abstract**

11 Accurate estimation of transpiration in individual trees is important for understanding plant

12 responses to environmental drivers, closing the water balance in forest stands and catchments,

13 and calibrating earth system models, among other applications. However, the cost and power

14 consumption of commercial systems based on sap flow methods still limit their usage. We

15 developed and tested a cost-effective (<\$150), simple to construct, and energy efficient sap flux

16 device based on the heat pulse method. Energy savings were achieved by reducing the voltage of

17 heat pulses and using an internal clock to completely shut down the device between pulses.

18 Device accuracy was confirmed by laboratory estimates of sap flow made on excised branches of

19 *Acer saccharum* and *Tsuga canadensis* (adjusted R^2 = 0.96). In a 174-d field installation of 12

20 devices, batteries (eight rechargeable Ni-MH AA) needed to be replaced every 14 days. Sap flux

21 measurements in the field tracked expected variations in vapor pressure deficit and tree

22 phenology. The low cost, compact design, reliability, and power consumption of this device

23 enable sap flux studies to operate with more replication and in more diverse ecological settings

24 than has been practical in the past.

25

26 **Key Words**
27 Sap Flux
28 Heat Pulse Velocity (HP)
29 Low-cost sensors
30

31

32

33

34

Specifications table	
Hardware name	J_s^5
Subject area	Environmental, Planetary and Agricultural Sciences
Hardware type	▪ Field measurements and sensors ▪ Electrical engineering and computer science
Open-Source License	GNU General Public License v3.0
Cost of Hardware	Complete unit: $109
Source File Repository	OSF: https://doi.org/10.17605/OSF.IO/KBZ5Y GitHub: https://github.com/justinbeslity/Js5-Novel_Sap_Flux_Device

36

1. Hardware in context

Canopy transpiration (E_c) from trees is the largest component of evapotranspiration (ET) in many habitats [1–3], and the measurement of E_C is critical to understanding vegetative, hydrologic, and meteorologic function in forested systems. Several methods have been developed to measure E_c, including sap flow measurements, weighing lysimeter, and eddy covariance [1,4–6]. Despite the wide application of these methods, they remain expensive, time consuming, and cumbersome to employ [7,8]. Advancement of sap flow methods offer perhaps the most promising route for simplifying implementation and reducing costs of Ec measurements. However, since sap flow measurements occur at the scale of a single tree, attempts to estimate E_c over a large area must involve the measurement of sap flow from multiple trees and at different radial depths in order to properly capture variations in transpiration due to tree size, species, and landscape position [9–12]. This poses a fundamental constraint for large scale transpiration scaling, as the required number of sap flow sensors is often prohibitively expensive if purchased from commercial retailers (i.e., $\geq$ $1000 per unit). Cost-saving options such as using centralized data loggers within plots make it difficult to select trees that adequately represent the study watershed, while commercial probes do not allow for sampling a wide range of radial depths or with different sap flux methods. In addition to cost, energy consumption is a concern. Sap flow installations away from the convenience of the electrical grid have traditionally used heavy and bulky lead-acid batteries, either replaced every few days or connected to solar panels [13–15]. The need for

56 frequent transport of bulky batteries places an additional logistical limit on the number of sensors

57 that can be deployed and limits the ability to monitor for extended periods.

58   To overcome these two primary constraints of cost and energy usage, we developed and

59 tested a prototype sap flow device, hereafter referred to as the J_s^5 (a play on the common

60 abbreviation for sap flux density and the developers' names), designed to be low cost (<$150),

61 adaptable, and to draw substantially less power than standard, existing commercial devices,

62 while maintaining a high degree of accuracy. Several recent attempts have been made to develop

63 custom-built devices to circumvent the need for commercial probes and dataloggers. Cárdenas et

64 at. (2019), Miner et al. (2017), and Jones et al. (2020) each developed sap flow units using cost-

65 efficient, microcontroller-based designs [16–18]. However, none of these devices implemented

66 measures to prolong battery life. Cárdenas et al. (2019) and Miner et al. (2017) reported that the

67 devices could run for several days to a week using a 12V lead acid battery and a 14.8V lithium-

68 ion battery respectively, which would limit field applications and require frequent battery

69 changes. Jones et al. (2020) powered their device using a 12V lead acid battery, and their device

70 has a nominal continuous power demand of 85mW. Additionally, none of these prior devices

71 demonstrated an ability to work over the range of expecting field conditions in trees.

72   Here, we describe the development and evaluation of two features to reduce power

73 consumption in sap flow sensors, including a) the minimum voltage of the applied heat pulse

74 necessary to accurately measure sap flux density (SFD), and b) the ability to use an internal

75 clock to allow for zero power consumption between measurements. In addition to the power

76 savings offered by this device, we demonstrate its flexibility by sampling across several radial

77 depths using two different sap flux methods. The overall effectiveness of the J_s^5 as well as the

78 power savings and reliability are evaluated using species of different xylem anatomy (*Tsuga*

79 *canadensis* [softwood], and *Acer saccharum* [diffuse-porous hardwood]) in both lab tests (using

80 excised branches) and field tests.

81

82 **2. Hardware description**

83 The J_s^5 consists of two main components: 1) probes used for generating and detecting heat

84 differences and 2) circuitry (Figure 1).

85

Figure 1: J_s^5 deployed in the field. The waterproof housing case contains both the printed circuit board, as well as the eight AA batteries used to power the device. The probes extend out of the bottom of the housing unit and are inserted into drilled holes in the tree. Mylar shielding is placed over the probes to reduce the influence of solar radiation. Photo credit: Justin Beslity.

2.1. Probes

All probes were constructed with 5 cm long stainless-steel dispensing needles. Reference probes (i.e., temperature sensor probes) were constructed from 1.27-mm diameter (18 gauge) needles,

94   and a 10K NTC thermistor was used for the temperature sensor (GA10K2MCD1, TE

95   Connectivity, Schaffhausen, Switzerland). Multiple thermistors can be placed within a single

96   dispensing needle to obtain multiple radial measurements across the same reference probe.

97   Thermistor resistance was converted to temperature using the Steinhart-Hart equation. Heating

98   probes were constructed by threading two loops of heater wire (36AWG [0.12-mm], TFCC

99   Insulated Thermocouple Wire, Omega Engineering Inc., Norwalk, CT, USA) through the needle

100 [16]. Approximately 25 cm of heater wire are required to construct a 5 cm long heater probe. All

101 probes were backfilled with epoxy (Omega Bond 101, Omega Engineering, Stamford, CT, USA)

102 once thermistors or heater wires were inserted.

103 *2.2. Circuitry*

104 The controller and data logger design are adapted from Miner et al. (2017) [16]. An ESP8266-

105 based microcontroller (Lolin D1 mini, WeMos Electronics) is used to operate the sap flow

106 probes. This microcontroller offers a cost-effective replacement to both the Campbell datalogger

107 and Arduino UNO in a compact size which could fit within a compact, custom, weather-proof

108 housing unit (Polycase, Inc.). Data is recorded using a micro-SD card inserted into a card reader

109 module connected to the microcontroller. A P-Channel MOSFET (IRF9540) and a real time

110 clock (RTC; DS3231) act as a switch to turn off the microcontroller, allowing for complete

111 system shutdown, a major power saving innovation [19]. The RTC maintains date-time

112 information with a separate 3.3V coin battery (CR2023) during system shut down. The input

113 voltage is moderated by the P-Channel MOSFET. The RTC square-wave output signal is used to

114 close the P-Channel MOSFET gate and complete the circuit during each sampling cycle. A N-

115 Channel MOSFET, controlled via the microcontroller, is used to operate the heater probes. Input

116 voltage is moderated via DC linear fixed voltage regulators to provide a constant and rated

117 output voltage. All components were mounted on a custom PCB and soldered in place. The entire

118 system is powered by eight AA Ni-MH rechargeable batteries.

119 *2.3. Software system*

120 The software system for the $J_s{}^5$ includes two separate programs, both coded with Arduino IDE

121 [20]. The first program sets the date and time on the RTC unit, as well initiates the SD card,

122 establishing the file to which the data will be written. The second program is designed to:

123   1. Initiate the microcontroller.

124   2. Collect baseline temperature measurements via the 10K NTC thermistors placed within

125   the reference probes.

126   3. Initiate the heat pulse (~ 2 s).

127   4. Monitor the subsequent temperature changes (~ 100 s).

128   5. Clear the alarm on the RTC to open the P-Channel MOSFET gate and power off the

129   device.

130   This sequence then repeats based on the two programable alarms set on the RTC. While a

131 30 minute sampling rate is common for sap flow measurements, the RTC can be programmed to

132 sample at more or less frequent rates [21–23].

133 **3. Design Files**

Design file name	File type	Open-source license	Location of the file
Gerber_Sap-Flux-System_SD-Card_8-Therms-042221_2022-03-21	Gerber	GNU General Public License v3.0	https://doi.org/10.17605/OSF.IO/KBZ5Y
Board_Configuration_SD.ino	INO	GNU General Public License v3.0	https://doi.org/10.17605/OSF.IO/KBZ5Y
Write-Sap-Flow-Code_SD_Card.ino	INO	GNU General Public License v3.0	https://doi.org/10.17605/OSF.IO/KBZ5Y

134

135   1. Gerber_Sap-Flux-System_SD-Card_8-Therms-042221_2022-03-21: The file used to

136   order designed printed circuit board via JCLPCB (PCB Prototyping and Manufacturing,

137   Guangdong Province, China).

138   2. Board_Configuration_SD.ino: The file used to program the RTC unit and initialize the

139   SD card.

140   3. Write-Sap-Flow-Code_SD_Card.ino: The file used to run sap flux measurment

141   operations.

142

143

144

145

146

147

148

149

150

151

152

153

154 **4. Bill of Materials**

Designator	Part	Number	Cost per unit - USD	Total Cost - USD	Distributer	Material Type
Thermistors	10K NTC Thermistor (GA10K3MCD1)	8	$2.89*	$23.12	Mouser	Thermistor
Microcontrollers	Lolin Wemos D1 Mini	1	$7.50	$7.50	Amazon	Non-specific
ADC	ADS1115	2	$6.00	$12.00	Amazon	Non-specific
RTC	DS3231SN	1	$3.60	$3.60	Amazon	Non-specific
2.5 V Reference	LT1460GIZ-2.5#PBF	1	$2.35*	$2.35	Mouser	Non-specific
6 V Regulator	L7806CV-DG	1	$0.31*	$0.31	Mouser	Non-specific
P-Channel MOSFET	IRF9540NPBF	1	$0.72*	$0.72	Mouser	Semi-conductor
N-Channel MOSFET	RFP30N06LE	1	$0.80*	$0.80	Amazon	Semi-conductor
MicroSD Card Adapter	MicroSD Card Adapter (HW-125)	1	$1.00	$1.00	Amazon	Non-specific
MicroSD Card	SanDisk Extreme 32GB microSD	1	$15.00	$15.00	Amazon	Non-specific
Battery Holders	8x AA Battery Holders	1	$8.18*	$8.18	Amazon	Non-specific
AA Batteries	Energizer Ni-MH 1.2 V 2.3 Ahr batteries	8	$1.88	$15.00	Amazon	Ni-MH
Lithium Coin Cell Batteries	Lithium CR2032 3 V batteries	1	$0.60	$0.60	Amazon	Lithium
Outer Protective Casing	WH-02 winged NEMA enclosure	1	$8.00	$8.00	Polycase	Non-specific
1K ohm Resistors	1K ohm resistors	1	$0.01	$0.01	Amazon	Resistor
10K ohm Resistors	10K ohm resistors	11	$0.11	$1.21	Amazon	Resistor
100k ohm Resistors	100K ohm resistors	1	$0.11	$0.11	Amazon	Resistor
Heater Wire	TFCC-005 PFA insulated wire	< 2 ft	$1.10	$1.10	Omega	Resistance Wire
Stainless Steel Dispensing Needle	75165A249	3	$0.56	$1.69	McMaster-Carr	Non-specific
Jumper Wires (red)	Hellotronics 15 cm M/M red	10	$0.12	$1.20	Amazon	Non-specific
Jumper Wires (black)	Hellotronics 15 cm M/M black	10	$0.12	$1.20	Amazon	Non-specific
Extension wire	24 AWG Low Voltage Red/Black bonded wire	~ 5 ft	$2.00	$2.00	McMaster-Carr	Insulated copper wire
Electrical Tape	Scotch 3M Electrical Tape	Small Amount	$1.00	$1.00	Amazon	Non-specific
Epoxy	OB-101-2	Small Amount	$0.30	$0.30	Omega	Non-specific
Heat shrink wrap	PPCLION 3/8 and 1/8 in 3:1 heat shrink wrap	Small Amount	$1.00	$1.00	Amazon	Non-specific

155

156 Pricing Notes:

157   * price will vary with distributor and purchase date

158

159 **5. Build Instructions**

160 The hardware needed to construct the J_s^5 is listed in the Bill of Materials. The device can be

161 separated into to two main components, 1) the probes, and 2) the printed circuit board (PCB)

162 (Figure 2). The probes and circuit board can be customized to meet the needs of a particular

163 study (i.e., number of radial measurement points, length of the probe, sampling frequency, and
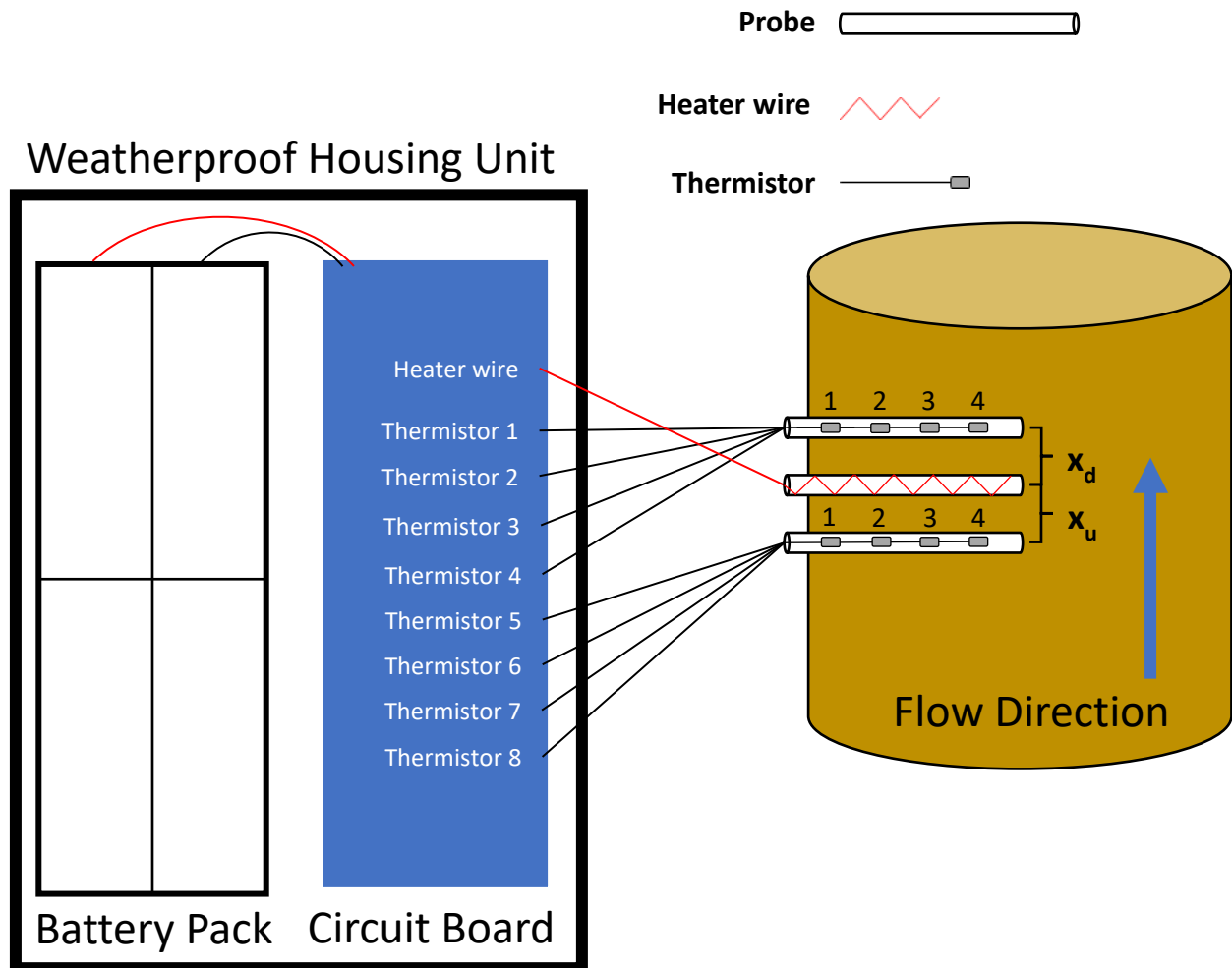
164 sap flow methodology).

Figure 2: Simplified schematic representation of the J_s^5. The thermistor numbers on the circuit board correspond to the numbers above the thermistors in the reference probes (i.e., temperature sensor probes). The circuit board is designed to accommodate eight thermistors, which allows for four measurement depths in most sap flow methods. The spacing between heater probe and the downstream (x_d) and upstream (x_u) reference probes can be adjusted to switch between different sap flow methods. The 8x AA battery holder and printed circuit board fit side by side within the waterproof housing unit (WH-02 winged NEMA enclosure).

5.1. Probes

Most commercial sensors include two radial measurement points along the length of the probe (e.g., Implexx Sap Flow Sensor, Implexx Sense, Melbourne, Victoria, Australia). At least two radial measurements are recommended when using the heat pulse velocity method, though specific experiments may require additional radial measurement points for more accurate measurements [24]. Here, the construction of a 5 cm reference probe with four radial

180 measurement points (0.5, 1.5, 2.5, 3.5 cm) will be detailed, as well as the accompanying 5 cm

181 heater probe.

182

183   1. <u>Reference Probe (i.e., temperature probe)</u>

184   a. *Cut dispensing needle to desired length (optional):* When measuring sap flow on

185   smaller diameter trees, it may be desirable to cut the dispensing needles to a

186   shorter length. Using either a hacksaw or a Dremel (recommended), cut the shaft

187   of the dispensing needles to the desired length. In this example, the entire 5 cm

188   length of the dispensing needle is used, and no cutting is required.

189   b. *Mark thermistor depth:* A 1:1 scale template, created with PowerPoint, depicting

190   the location of each thermistor bead within the dispensing needle is

191   recommended to accurately place thermistors (Figure 3). Using the PowerPoint

192   template, align the thermistor bead at the corresponding depth, making sure to

193   account for the length of the dispensing needle base (1.8 cm), and mark the lead

194   wires using a fine point white out pen (Figure 4). Repeat this process for each

195   thermistor at each depth.

Length of heater wire

1 cm — Thermistor 4
1 cm — Thermistor 3
1 cm — Thermistor 2
0.5 cm — Thermistor 1
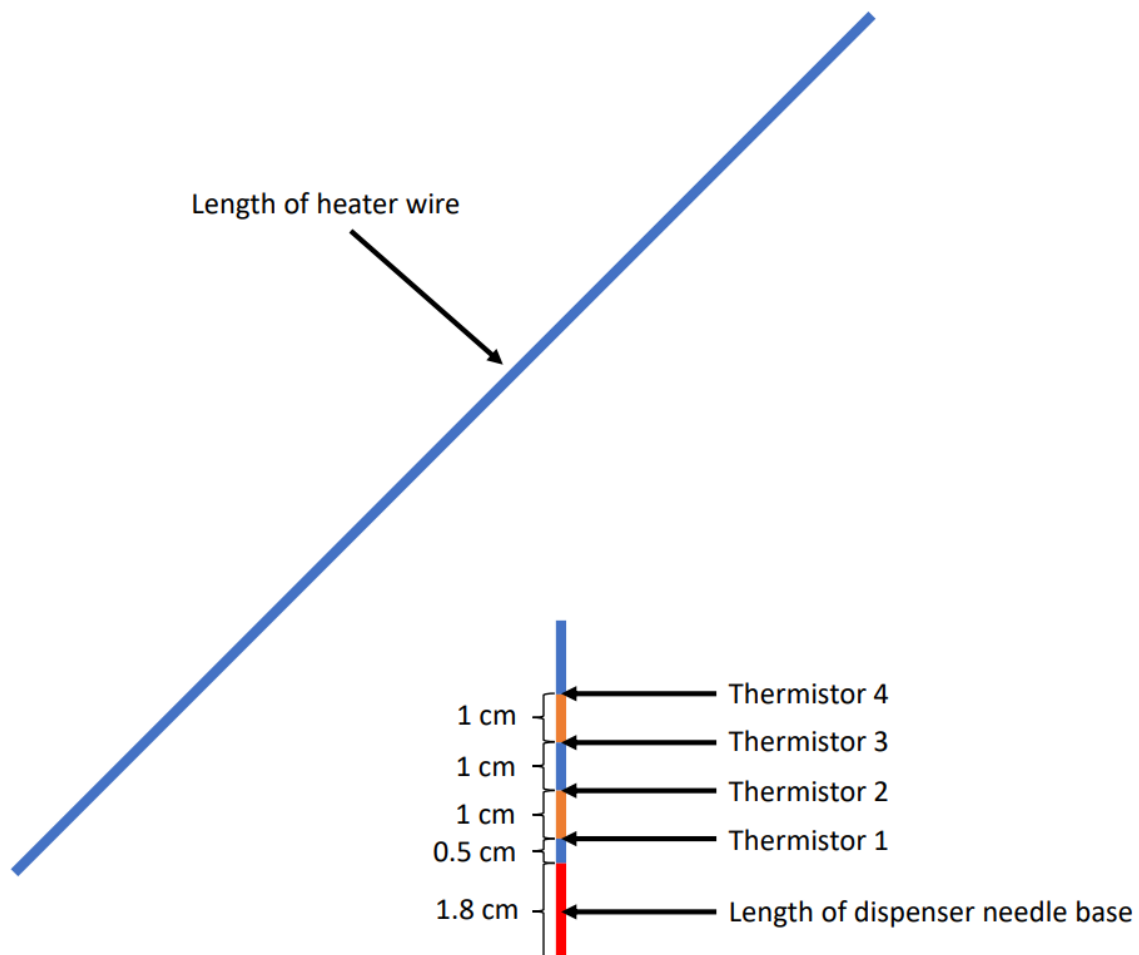1.8 cm — Length of dispenser needle base

Figure 3: PowerPoint template of thermistor placement withing dispensing needle and the necessary length of heater wire needed for the corresponding heater probes. The placement of thermistors is dependent on the needs of the user and should be adjusted depending on the intended use. Typically, at least two thermistors at different radial depths are recommended. Figure not to scale.

204
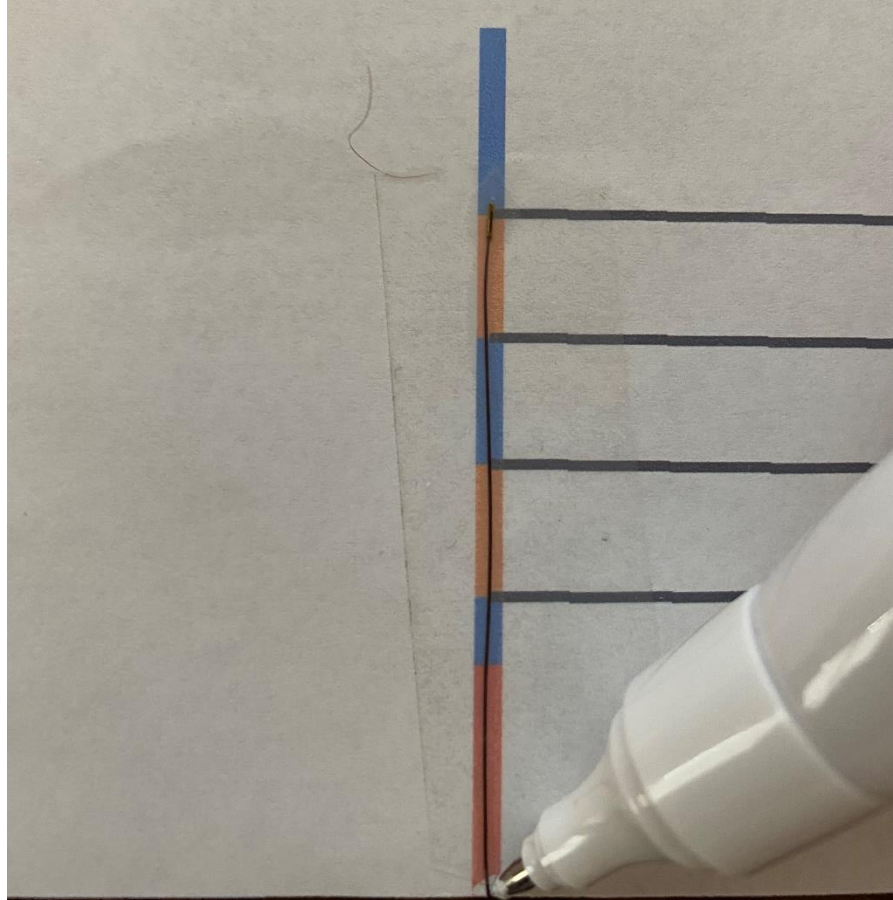
Figure 4: Marking the thermistor using white out pen. The thermistor bead has been positioned at the mark corresponding to "Thermistor 4" on Figure 2. The thermistor was taped down for this picture, and this is not recommended during construction. Multiple thermistors can be marked concurrently to expedite this step.

    c. *Align thermistors in dispensing needle:* Starting with the thermistor located at the deepest point within the dispensing needle (in this example, Thermistor 4), insert the thermistors through the base of the dispensing needle and align the applied white out mark of each thermistor with the edge of the bottom of the base (Figure 5). Once each thermistor is properly placed, apply a tiny bead of super glue to temporarily hold the thermistors lead wires in place. Allow time to dry.

11
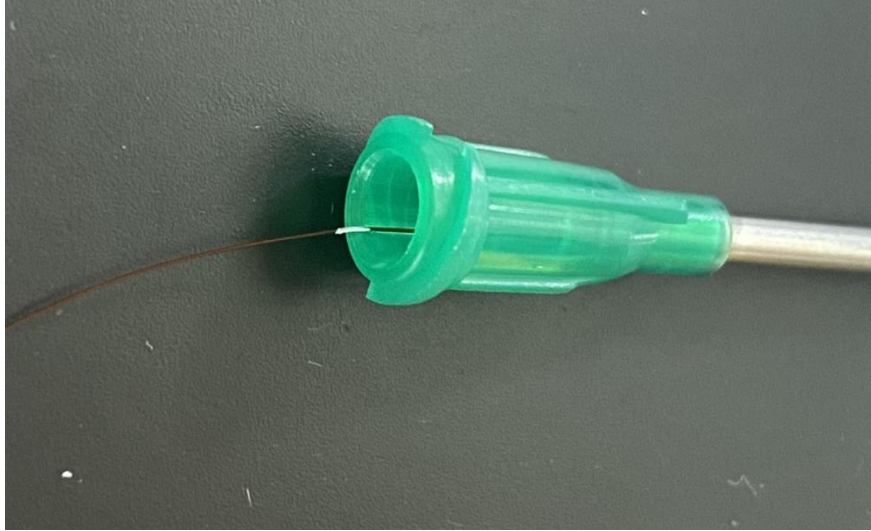
Figure 5: Aligned thermistor in dispensing needle. Note the applied white out mark aligned with the edge of the bottom of the dispensing needle base.

    d. *Prepare epoxy:* When ready, mix equal portions of the Omega Bond 101 resin and hardener in a weigh boat. Epoxy will become difficult to work with after one hour and completely sets in 24 hours.

    e. *Dispense epoxy:* Load the 1 mL syringe with epoxy and firmly insert the tip of the syringe into the base of the prepared dispensing needles. The super glue will provide some security, but it may be helpful to bend the thermistor lead wires back upon the dispensing needle base and hold them in place (Figure 6.a). Dispense epoxy until a small amount emerges from the tip of the dispensing needle. Remove the excess epoxy from the tip of the needle, ensuring that the length of the metal shaft is free from epoxy. Very gently, work the syringe tip out of the base of the dispensing needle. Fill in the base with additional epoxy (Figure 6.b). Take care to keep the thermistor lead wires free of epoxy. Let cure for 24 hours.
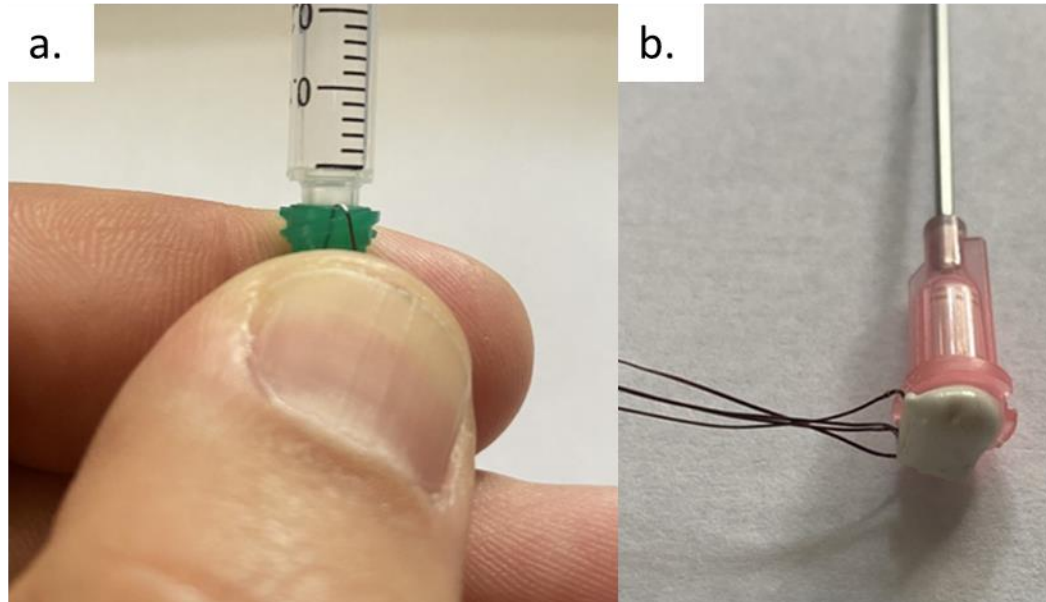
234

Figure 6: Applying epoxy through the base of the dispensing needle. While the small amount of super glue applied in section c. *Align thermistors in dispensing needle* will keep the thermistors secured to the base, it may be helpful to bend the thermistors back against the base of the dispensing needle when inserting the 1 mL syringe into the base of the syringe, as seen in Figure 6.a. After observing the epoxy emerging from the tip of the needle, and while continuing to hold the thermistors in place, gently work the syringe tip out of the base of the dispensing needle and apply additional epoxy to fill the base of the dispensing needle, as seen in Figure 6.b.

A

f. *Attach extension wire to thermistor leads:* Once the epoxy has cured, separate the two lead wires of each thermistor (notice the small, uninsulated ends of each lead wire). Thermistors can be identified by the length of the lead wires protruding from the base of the dispensing needle (Figure 7). Using a small piece of duct tape as a label, number four ~ 60 cm segments of 24 AWG low voltage bonded extension wire from one to four corresponding with the thermistors in the dispensing needle (Figure 8). Labeling the bonded extension wire corresponding to the connected thermistor is critical as there is no simple way to differentiate the thermistors once the probe has been completed. Strip the ends (~ 0.5 cm) of each segment of bonded wire, place a 1 cm piece of the 1/8 in diameter shrink wrap on the bonded wire, firmly wrap the thermistor lead wire around the exposed bonded wire. Solder the exposed lead of the thermistor and the bonded extension wire together, move the small piece of heat shrink wrap over the exposed wire, and use a heat gun to seal the connection (Figure 9). Alternatively, electrical tape can be used to insulate the connections. Repeat this process for each thermistor.

13

257

258
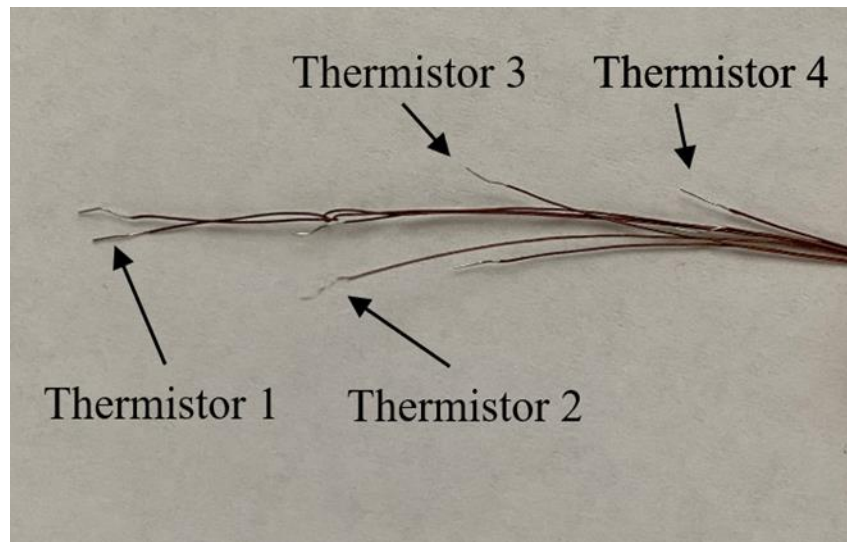
Figure 7: The leads of four thermistors after sealing the base of the dispensing needle with epoxy. Note that the depth order of the thermistors can still be determined after dispensing needle is epoxied (refer to PowerPoint template).

262
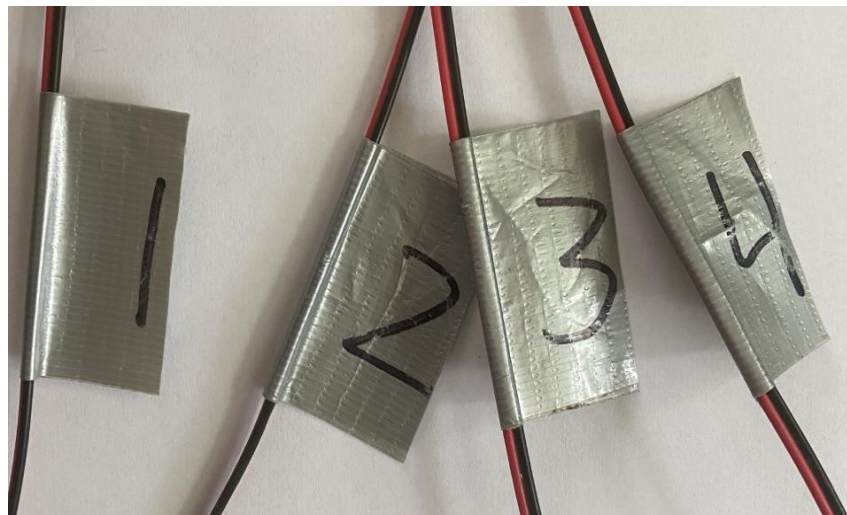
263
Figure 8: Labeled bonded extension wire. Each labeled extension wire corresponds with the thermistor number in Figure 7.
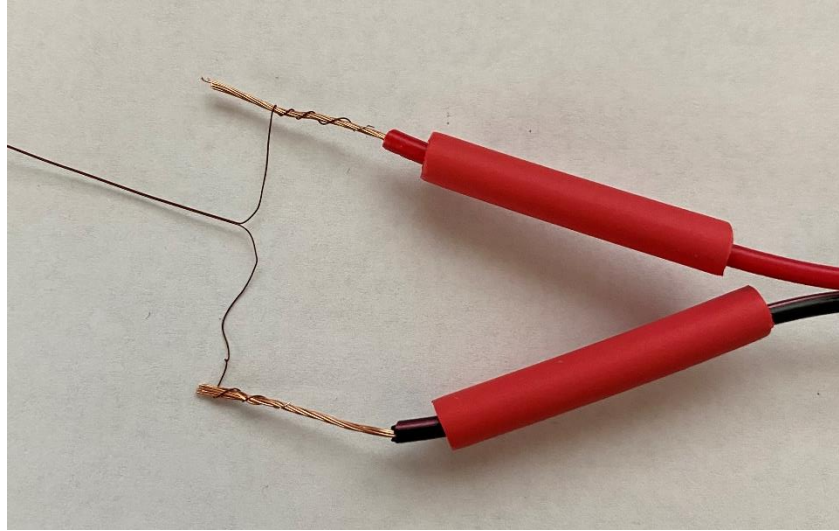
266

267

Figure 9: Connecting the thermistor leads to bonded extension wire. If using heat shrink wrap, be sure to put in place before soldering the thermistor leads to the bonded extension wire.

270

271   g. *Secure Probe:* Using either the 3/8 in heat shrink wrap or electrical tape, sheath the

272   probe from the base of the dispenser needle past the soldered connections to create a

273   robust and secure probe for deployment (Figure 10).

274

Figure 10: Completed reference probe with heat shrink wrap sheath. At this point, the only way to identify the thermistors is the labeling on the bonded extension wire.

277

278   2. <u>Heater probes</u>

279   a. *Cut dispensing needle to desired length (optional):* The dispensing needles for

280   the heater probes should be cut to match the length of the reference probes.

281   b. *Cut heater wire to length:* Using the PowerPoint template, cut a ~ 25 cm length
282   of heater wire.
283   c. *Double loop:* First fold the heater wire segment in half and then fold ~ 5 cm
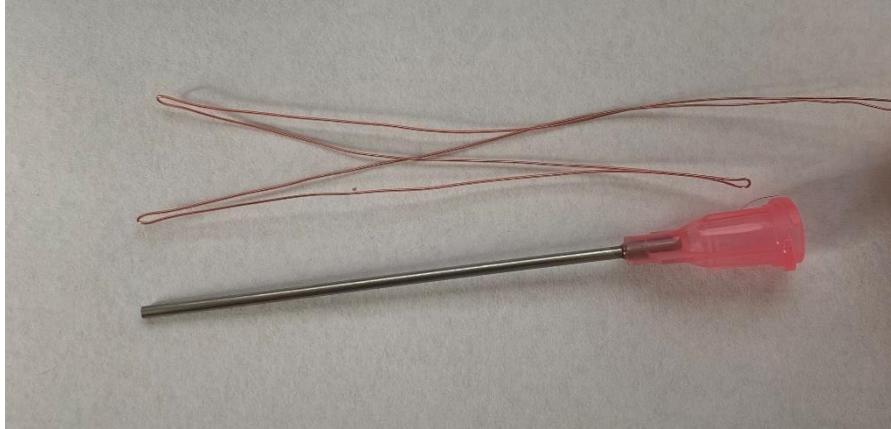284   back on itself, creating a "double loop" (Figure 11).

285
286 **Figure 11:** The "double loop" of heater wire prior to insertion into the dispensing needle.
287

288   d. *Insert heater wire:* Beginning from the metal tip of the dispensing needle, insert
289   the two ends of the heater wire segment and slowly push the heater wire through
290   the needle. The fit should be tight, but manageable. Be sure to strip the two ends
291   of the heater wire before soldering them to the bonded wire (Figure 12). Excess
292   heater wire should be removed to decrease the overall power demand of the
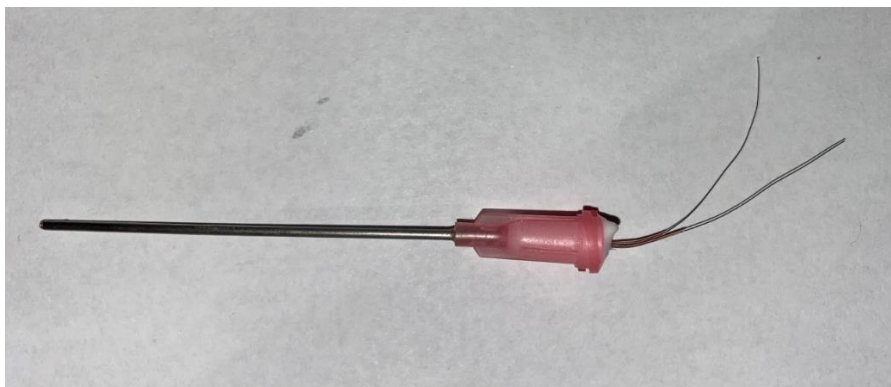293   heater probe.

294
295 **Figure 12:** Epoxied heater probe. Note the stripped ends of the heater wire.
296

297   e. Follow steps d-g from the previous section to complete the heater probes.

298

299

16

300   *5.2. Circuitry*

301   The circuitry (Figure 13) is mounted on a fabricated PCB. The Gerber file listed in the design

302   files table includes a silk layer marking the location of each hardware component (Figure 14).

303   Each board is designed to operate up to eight individual thermistors and two heater probes. In

304   this example, we connect two four-thermistor probes and one heater probe to the printed circuit

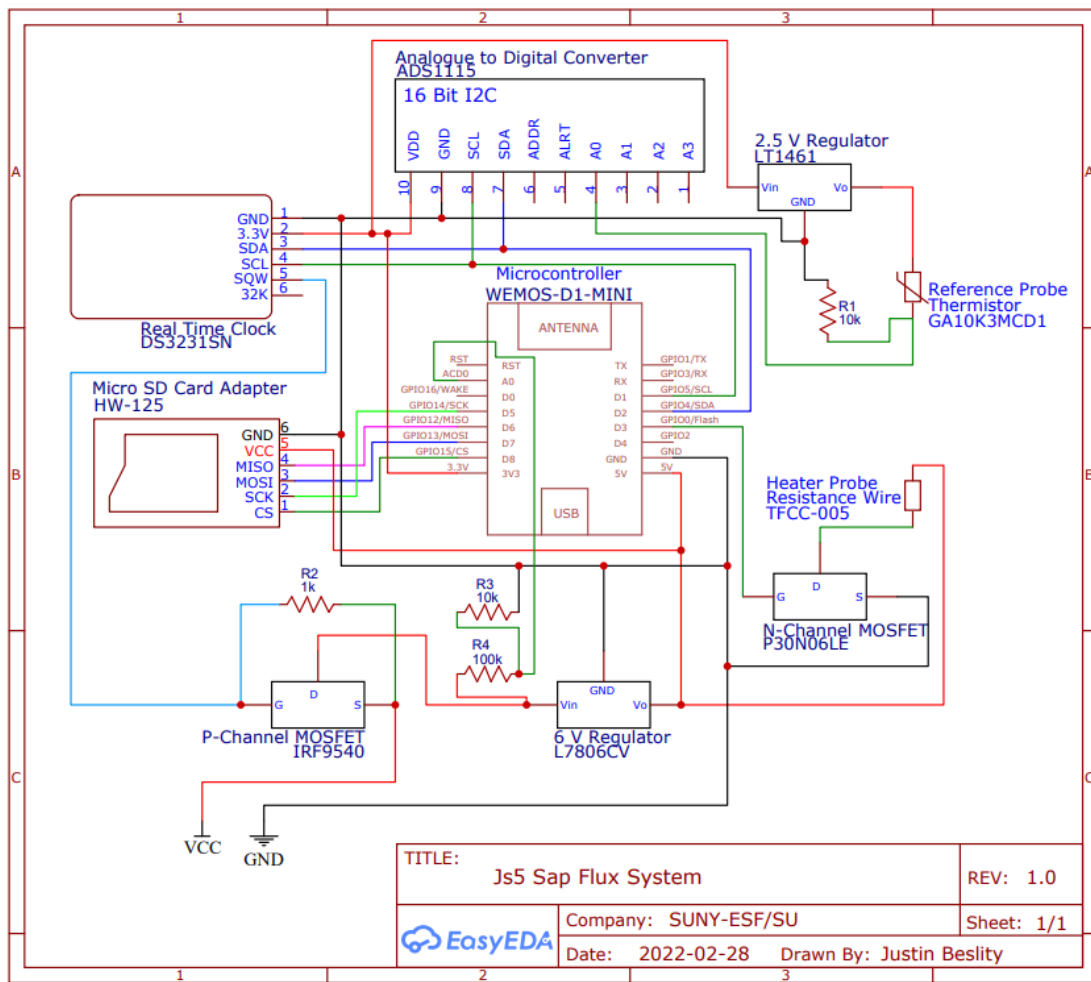305   board. Most heat pulse velocity methods require both an upstream and downstream reference

306   probe.

307

308

309   **Figure 13:** Simplified J_s^5 circuit schematic.
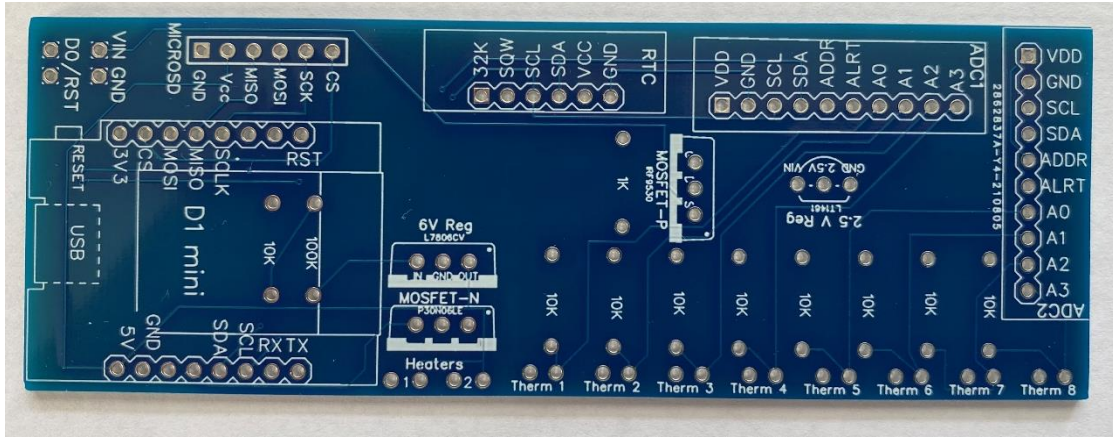
310

311

312

313

Figure 14: Printed circuit board for the J_s^5 showing the silk layer with annotated locations for each hardware component.

The recommended method to assemble the circuit boards is as follows:

    1. *Resistors:* Place the one 1k, nine 10k, and one 100k Ohm resistors in their respective positions and solder in place (Figure 15). Refer to the silk layer on the PCB when placing the resistors.
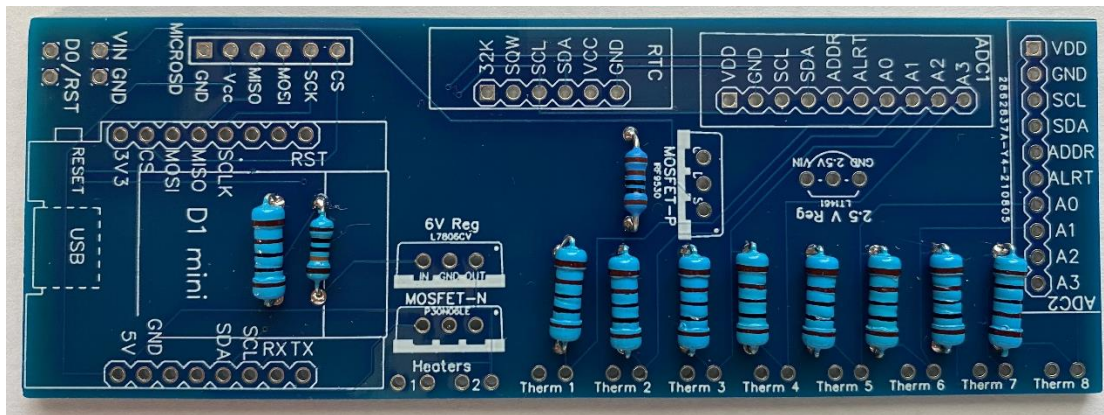

321

Figure 15: Printed circuit board with resistors in place.

    2. *RTC modification:* The RTC DS3231SN requires slight modification to function as the alarm system for the J_s^5 [19]. Using the tip of the soldering iron, gently remove the resistors identified in Figure 16.
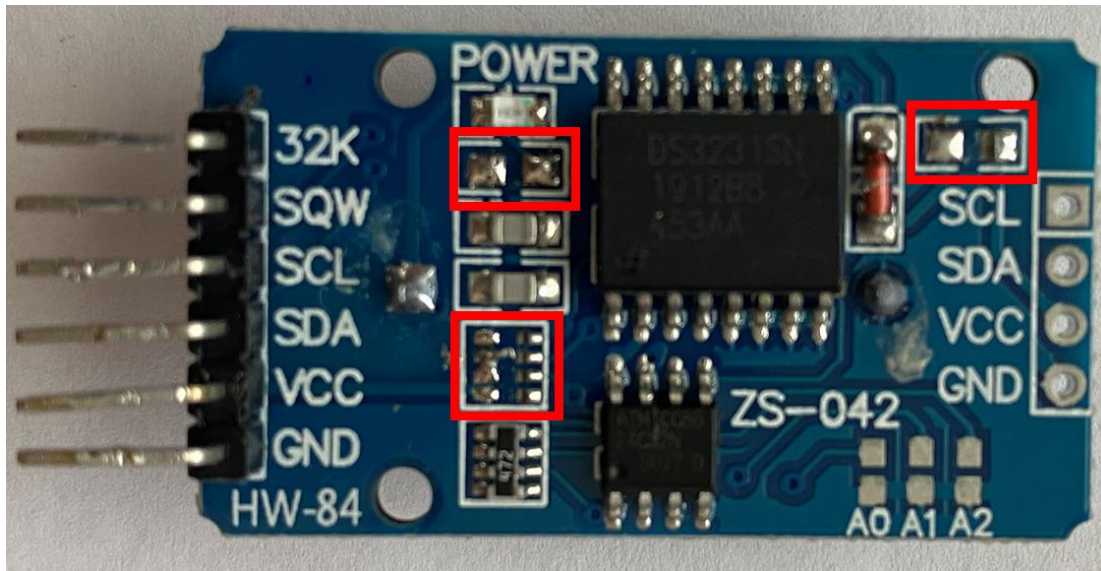
18

327

Figure 16: Modified RTC DS3231. Resistors (boxed in red) than need to be removed for the RTC to function as the alarm system for the J_s[5].

3. *Components:* Place the two ADC1115 and solder in place, followed by the microcontroller (D1 mini), P and N-Channel MOSFETs, 6 V linear voltage regulator, 2.5 V voltage regulator, modified RTC DS3231SN, and finally the micro-SD card adapter module (Figure 17).
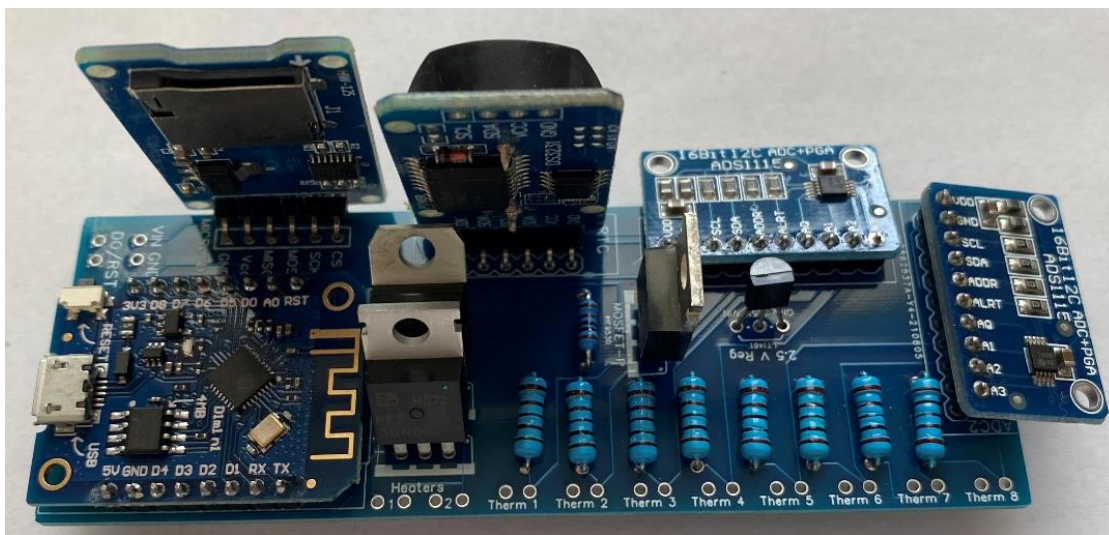

335

Figure 17: Printed circuit board with all hardware in place.

4. *Clean up:* Trim the leads of the resistors and other hardware components to create as flush a surface on the bottom of the PCB as possible. Be sure to avoid any potential electrical shorts (Figure 18).
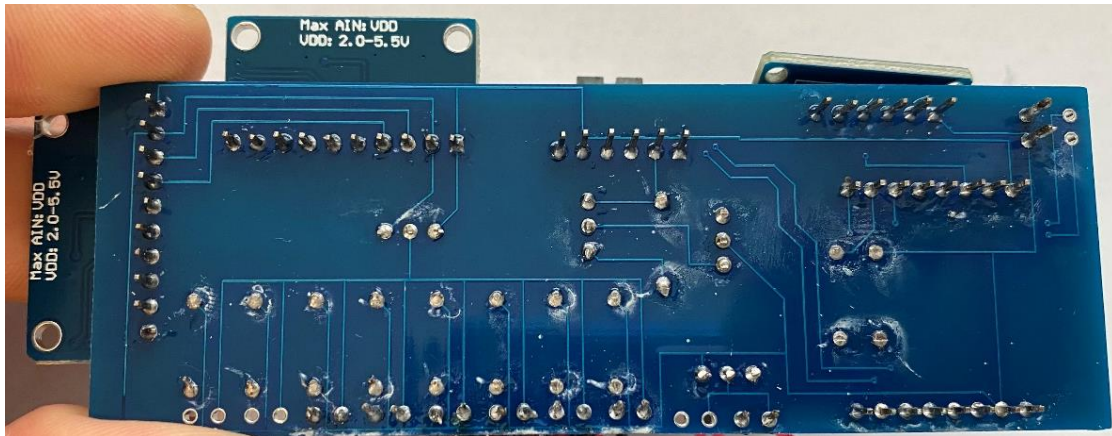
19

341

Figure 18: Printed circuit board with all hardware leads trimmed to prevent electrical shorts.

342
343

5.3. Completing the Device

1. *Attach probes to the PCB:* The thermistors in the probe attach to the circuit board so that thermistor 1 in the first probe is connected to the "Therm 1" pin holes, and thermistor 1 on the second probe is connected to "Therm 5" pin holes (thermistor is abbreviated as "Therm" on the printed circuit board; see Figure 2). Strip away the insulation at the two ends of the extension wire opposite the dispensing needle. The exposed ends can be directly soldered to the printed circuit board, though we have found that the jumper wires listed in the bill of materials provided a robust connection to the circuit board which were able to withstand a full 7-month deployment in the field (Figure 19). Compact connectors can be incorporated between the jumper wires and the extension wire to allow for easy replacement in the case of probe or circuitry malfunction (Figure 20).

356
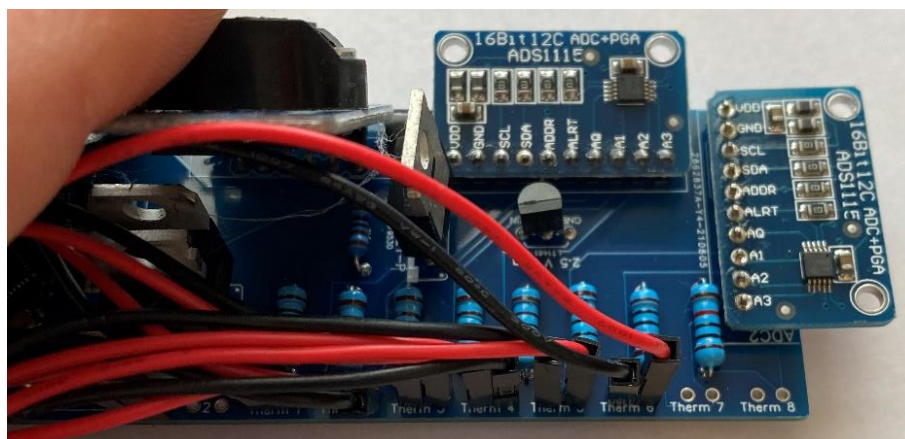
Figure 19: Connecting probes to the PCB.

20

358
359

360

Figure 20: Compact connectors attached to each length of extension wire. If a probe or PCB malfunctions in the field, these connectors allow for easy replacement of the defective part.

2. *Batter Holder:* Solder black and red jumper cables to the corresponding leads of the 8x AA battery holder. Cover connections with heat shrink wrap. Solder the red and black jumper wires to the Vin and GND pins on the PCB, respectively (Figure 21).

368

Figure 21: Connecting battery holder to the PCB.

370

371   3. *Drill an opening in the housing unit:* Using a 7/8 in hole saw drill bit, create an

372   opening in the bottom of the Polycase housing unit (Figure 22). Thread the probes

373   through the hole and place the PCB and battery pack side by side within the

374   housing unit.

375

Figure 22: Housing unit (Polycase WH-02) with 7/8 in hole drilled in the bottom.
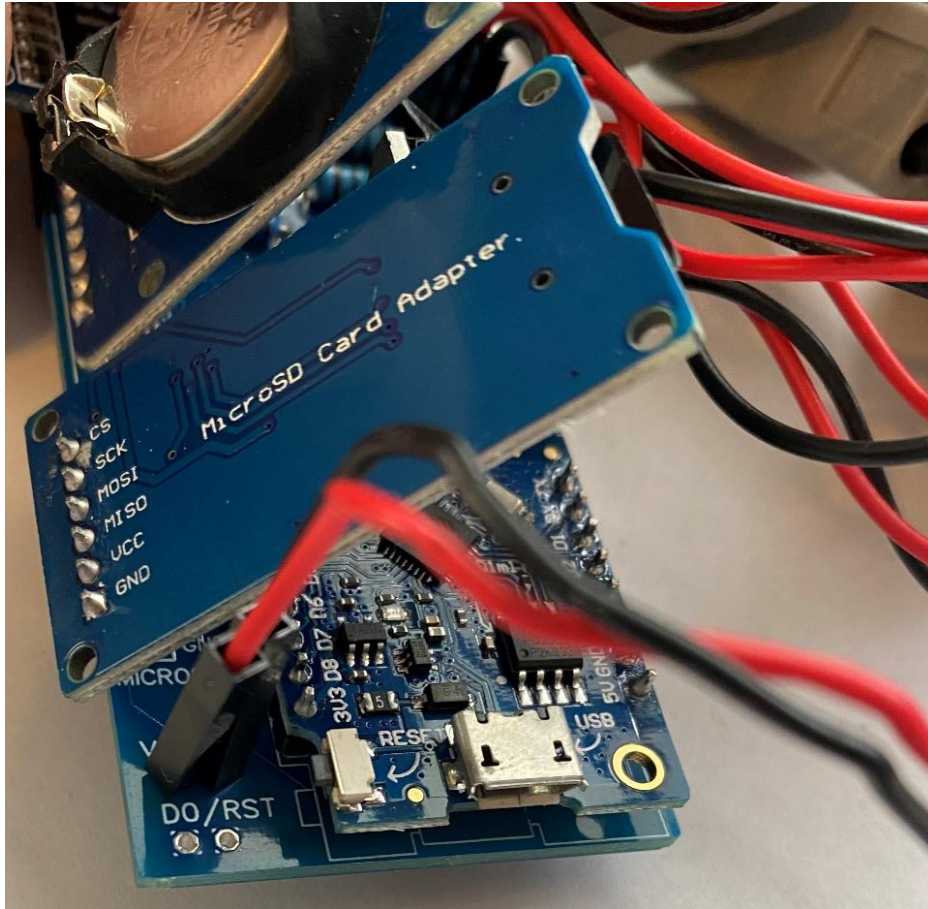
377

378   4. *Sealing the opening:* Seal the opening in the bottom of the housing unit with a small piece of poster tack, wrapping it around the extension wire and pressing it tight.

6. Operation Instructions

6.1. Programing

The $J_s{}^5$ requires two programs to operate, the first to set the time on the RTC, as well as to format the files to be written to during operation, and a second which controls the measurement cycle.

1. Install Arduino IDE for your operating system (https://www.arduino.cc/en/software)
2. Open Arduino IDE
3. Go to File > Preferences
    a. In the Preferences pop up menu, copy the following into the "Additional Board Manager URLs" textbox.

http://arduino.esp8266.com/versions/2.3.0/package_esp8266com_index.json

4. Open Boards Manager from Tools > Board > Board Manager… menu

393   a. Type "esp8266" into the text box.

394   b. Select esp8266 by ESP8266 Community and click "Install".

395   c. Exit the Board Manager menu.

396   5. Open Tools > Board > ESP8266 Boards (2.7.4) and select your specific ESP8266 (e.g.,

397   Wemos D1 mini)

398   6. Open Tools > Manage Libraries… and download the following libraries by typing the

399   names below into the textbox on the Manage Libraries… menu and clicking "Install".

400   a. Adafruit ADS1X15 by Adafruit

401   b. RTClib by Adafruit

402   c. SD by Arduino, SparkFun

403   d. uRTCLib by Naguissa

404   7. Select the correct port in the Tools menu

405   8. Upload the Board_Configuration_SD program to the microcontroller using the Arduino

406   IDE interface. Immediately upon upload, open the serial monitor to ensure the time is set

407   properly and the SD card has initialized.

408   9. Upload the Write-Sap-Flow-Code_SD_Card program to the microcontroller. Once

409   uploaded, and after the 5 second baseline temperature measurement, the LED on the

410   microcontroller should light up for ~ 2 seconds, indicating a heat pulse has initiated.

411   Check the heater probe to see if heat has been generated.

412   10. Take out the micro-SD card and check the data to ensure all thermistors are operational.

413

414   The duration of the heat pulse, as well as the baseline and post heat pulse temperature

415 measurements can be adjusted in the Write-Sap-Flow-Code_SD_Card.ino program.

416

417   *6.2. Installation*

418 To install the J_s^5 in mature trees follow the protocol below:

419   1. Remove a small portion of the bark from the tree at breast.

420   2. Using a drilling template and the drill bit listed in the bill of materials, carefully drill the

421   necessary holes in an area where the bark has been cleared. Number of holes, distance

422   between holes, and depth of holes will depend on the method chosen. Improper drilling of

423   holes is a common source of error [25].

424   3. Secure the housing unit to the tree within a close distance of the holes.

425   4. Apply the dielectric grease to the probes and carefully insert them into the tree.

426   5. Cover the probes with mylar shielding (see Figure 1).

427

428   *6.3. Heat Pulse Methods*

429   We tested our device, both in the laboratory and in the field, using the heat pulse (HP) method,

430   including the Tmax and heat ratio variants of the heat pulse method.

431   Heat-pulse methods - based on the fundamental conduction-convection equation

432   presented by Marshall (1958) - offer an alternative to the more commonly used thermal

433   dissipation methods. Heat pulse methods measure the velocity (V_h) of a short heat pulse (~2 s)

434   which can then be converted to SFD and whole-tree flow based on the physiological parameters

435   of the sap wood. The approach assumes heat is conducted from a central heater probe down the

436   tree to the "upstream" probe, and both conducted and convected up the tree to the "downstream"

437   probe. Heat pulse velocities typically range from -20 to 200 cm hr^{-1} in the field, though values up

438   to 500 cm hr^{-1} have been recorded in *Eucalyptus mannifera* [26].

439   There are several heat pulse methods, each with their strengths and drawbacks [27]. We

440   used the Dual Method Approach (DMA) to gauge the devices' capacities for measuring a wide

441   range of flows [28]. This method combines the Heat Ratio Method (HRM), capable of measuring

442   low/reverse flows, with the Tmax method, capable of measuring mid/high flow rates. The HRM

443   utilizes two sensor probes installed at equal distances up- and downstream of the heater probe to

444   determine the heat velocity with the equation:

445
$$V_{h,HRM} = \frac{k}{x} \ln\left(\frac{\Delta T_d}{\Delta T_u}\right)$$
Eq. 1

446   where $V_{h,HRM}$ is the heat velocity (cm s^{-1}), k is thermal diffusivity (cm^2 s^{-1}), x is the distance

447   between the sensor probes and the heater probe (cm), and ΔT_d and ΔT_u are the changes in

448   temperature upstream and downstream following the heat pulse (K), usually recorded at between

449   60 and 100 seconds [29]. This method has been further modified to account for differences in the

450   positioning of probes and heat pulse duration [30]:

451
$$V_{h,HRM} = \frac{2k\left(ln\left(\frac{\Delta T_d}{\Delta T_u}\right)\right)}{x_d + x_u} + \frac{x_d - x_u}{2\left(t - \left(\frac{t_o}{2}\right)\right)}$$
Eq. 2

452 where t_o is the heat pulse duration and x_d and x_u are the distances between the heater probe and

453 the down- and upstream sensor probes, respectively (see Figure 2).

454 The Tmax method utilizes one downstream sensor probe with the equation:

455
$$V_{h,Tmax} = \frac{\sqrt{x_d^2 - 4kt_m}}{t_m}$$
Eq. 3

456 where $V_{h,Tmax}$ is the heat velocity (cm s^{-1}), x is the distance between the heater and downstream

457 sensor probe, and t_m is the elapsed time (s) for the downstream sensor to reach the maximum

458 temperature of the heat pulse [31]. As with the HRM, this method has been modified to account

459 for differences in the heat pulse duration [32]:

460
$$V_{h,Tmax} = \sqrt{\frac{4k}{t_o} ln\left(1 - \frac{t_o}{t_m}\right) + \frac{x_d^2}{t_m(t_m - t_o)}}$$
Eq. 4

461 The heat pulse velocity selected for the DMA is determined by the Pérclet number (β)

462 defined as:

463
$$\beta = ln\left(\frac{\Delta T_{d,max}}{\Delta T_{u,max}}\right)$$
Eq. 5

464
$$If\ \beta\ \leq 1\ Then\ V_h = V_{h,HRM}$$

465
$$Else\ V_h = V_{h,Tmax}$$

466 where $\Delta T_{d,max}$ and $\Delta T_{u,max}$ are the difference between the pre-heat pulse and maximum post-heat

467 pulse temperatures in the down- and upstream probes, respectively [26].

468 Wound corrections for these methods are widely established, allowing for more accurate

469 results [29,33]:

470
$$V_c = BV_h$$
Eq. 6

471 where B is a correction coefficient that corresponds to a specific wound size. Pulse velocity is

472 converted to sap flux density (g cm^{-2} s^{-1}), using measured properties of the wood [34]:

26

$$SFD = \frac{\rho_b}{\rho_s}\left(m_c + \frac{c_{dw}}{c_s}\right)V_c \qquad \text{Eq. 7}$$

where ρ_b is the dry wood density (g cm^3), m_c is the moisture content (g$_{water}$ g$_{dry\ wood}^{-1}$), c_{dw} is the specific heat capacity of the dry sap wood material (J g^{-1} K^{-1}), and c_s and ρ_s are the specific heat capacity of sap and the sap density, often assumed to be the specific heat capacity and density of water, respectively.

Single point SFD measurements are converted to whole tree sap flow (F, g s^{-1}) by weighting each measurement from each temperature sensor by the corresponding sapwood area [24]:

$$F = \sum_{j=1}^{n} \pi\left(r_j^2 - r_{j-1}^2\right)SFD_j \qquad \text{Eq. 8}$$

where j is the number of temperature sensors in each probe and r is the radius associated with the jth temperature sensor.

7. Validation and characterization

7.1. Laboratory set up

Excised branches 5 to 8 cm in diameter were harvested from *Acer saccharum* (diffuse-porous) and *Tsuga canadensis* (softwood) at Hammond Hill State Forest (Dryden, NY). Branches were enclosed in a plastic bag with wet paper towel in the field to minimize cavitation. Immediately before the experiments, the branches were cut again under water to approximately 30 to 60 cm in length using a handsaw. It is possible that the length of some vessels exceeded that of the branch segments, though this would not impact the relationship between SFD and gravimetric flow rate once the vessels were recharged via positive pressure. The ends of each segment were shaved with a razor blade to remove potential damage to the xylem caused by the handsaw.

Sap flow was artificially generated in the laboratory by applying positive pressure to the branches. A 38 L pressure tank was partially filled with tap water, allowed to equilibrate to room temperature, and then pressurized using a hand pump. Pressure was maintained at near constant levels during experiments; periodic hand pumping throughout the experiment maintained pressure as measured with a digital pressure gauge (DPGA-05, Dwyer Instruments, Inc., Michigan City, IN, USA). The branch was secured to the canister using a rubber coupling and hose clamps. When the system was pressurized, water emerged only at the cut end of the branch,

501 and flow rate was measured gravimetrically based on the water collected in five-minute time
502 intervals. The J_s^5 was tested at four flow rates associated with 1, 3, 5, and 9 psi (induced by
503 changing positive pressure), as well as a no flow condition. Measurements at each flow rate were
504 repeated four or five times at each flow rate, depending on the ability to maintain a near constant
505 flow rate, to quantify precision.

506 The probes were inserted perpendicularly to the surface of each branch to a depth of 3
507 cm. Temperature sensors were positioned at 0.5, 1.5 and 2.5 cm along the upstream and
508 downstream reference probes to provide a weighted average sap flow rate. Bark was removed
509 from the area the probes were inserted to ensure as much of the probe as possible was in the sap
510 wood region. The reference probes were installed 0.5 cm up- and downstream of the heater probe
511 using a custom drill template. Dialectic grease was used to ease the insertion and to improve
512 contact between the probe and sapwood. The branch was held in a vertical position using a ring
513 stand to prevent any preferential flow patterns possible when positioned horizontally. Before
514 beginning experiments, water was run through the branch for approximately 10 minutes to allow
515 the branch temperature to equilibrate with the water temperature.

516 The lab experiment included: 1) sampling the baseline temperature measurements for 5
517 seconds, 2) applying a 2-second heat pulse (typically 6 V) [16,35], and 3) monitoring the heat
518 pulse for 100 s at 0.5 s intervals. The mean moisture content (m_c) and sapwood density (ρ_b) from
519 stem cores for *A. saccharum* and *T. canadensis* collected in the field were used to calculate the
520 predicted SFD from the heat pulse velocity (V_c) for each species. The SFD (g cm^{-2} s^{-1})
521 measurements were then converted to sap flow (g s^{-1}). The correlation between the predicted and
522 gravimetric sap flow was evaluated using linear regression statistics.

523 Following each branch experiment, Safranin O solution (0.1%) was added to the pressure
524 canister to obtain a measurement of sap wood area. The dye took approximately 5-15 minutes to
525 pass through the branch, depending on the species. A small cookie was then cut from the stem
526 segment and shaved with a razor blade. The cookie was scanned, and the area and depth of red
527 dye was determined using Image J software (Image J, NIH, USA, http://rsbweb.nih.gov/ij/). This
528 procedure was repeated for three branches from both species.

529

530

531   *7.2. Power Consumption*

532   To assess possible reductions in power consumption, a subset of runs on excised branches was

533   conducted using heat pulses applied at both 6 V and 12 V. When assessing the device at 12 V,

534   the L7806CV linear voltage regulator was replaced with a L7812CV linear voltage regulator (a

535   12 V linear regulator), and the number of batteries used to power the device was increased

536   accordingly. Flow rates were varied between 0 and 2500 g hr^{-1} with 25 to 30 measurements made

537   across the range for each branch. Estimated sap flow was compared to gravimetric sap flow for

538   both the 6 V and 12 V sets of measurements to evaluate change in accuracy as the voltage is

539   decreased. Heat pulses were applied for 2 s at both voltages. In accordance with Ohm's Law and

540   Joule's Law, halving voltage was expected to lead to one-quarter the wattage drawn.

541   The sap flow predicted by both 6 V and 12 V pulses were comparable with no clear

542   difference between them and a similar accuracy when evaluated against measured gravimetric

543   flow (Figure 23). The mean absolute errors of the predicted versus the measured values at 6 and

544   12 V were 201.1 (n = 25) and 278.8 (n = 30) g hr^{-1}, respectively. The adjusted R^2 for the

545   correlation between the predicted and gravimetrically measured sap flow was 0.97 and 0.93 for 6

546   and 12 V, respectively. Given the similarity in predicted sap flow, 6 V pulses were presumed as
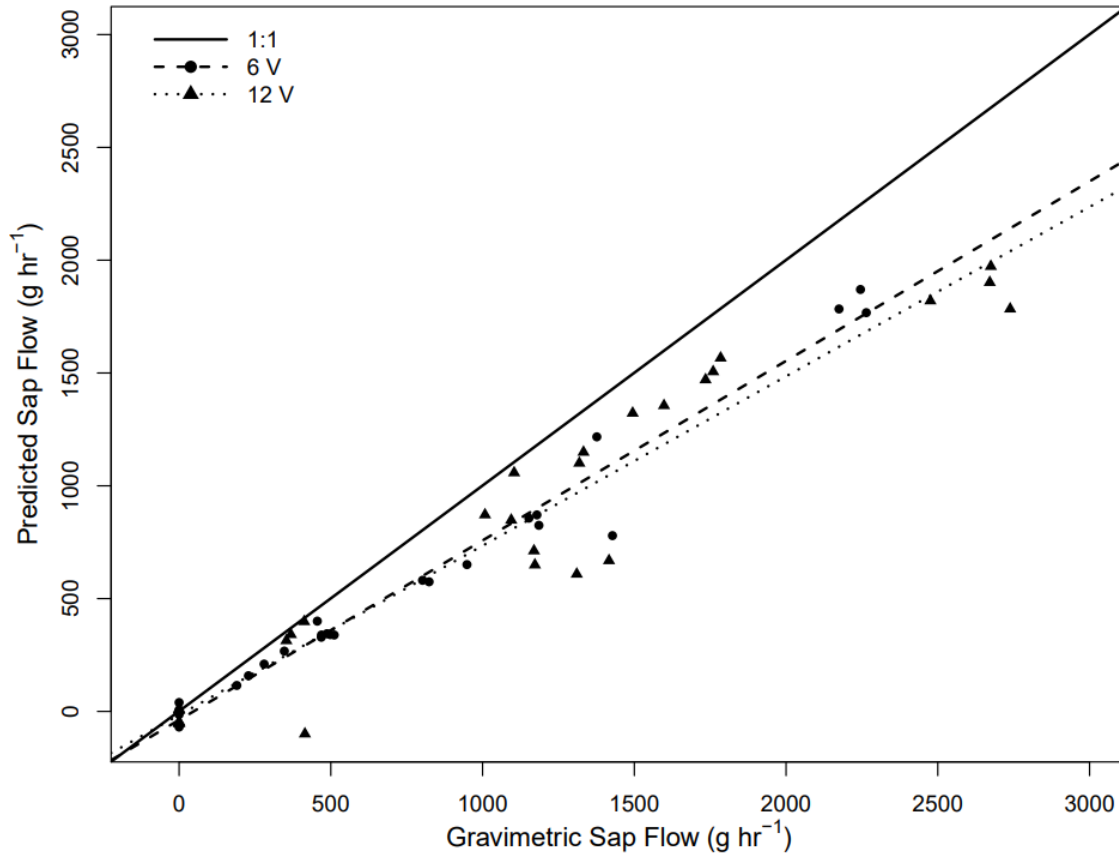
547   suitable as 12 V pulses.

Figure 23: Correlation between the predicted sapflow measure at 12 V (triangles) and 6 V (circles) versus the gravimetric flow rate. The solid line represents a 1 to 1 relationship and the dashed and dotted lines represents the linear regression between the predicted and gravimetric sap flow for 6 and 12 volts, respectively.

Device power usage was evaluated in order to quantify the period of time the system could be operated on a single battery charge (presuming 5 s of baseline temperature assessment, 2 s of heating, and 100 s of pulse monitoring). The Arduino based microcontroller drew 0.03 A during operation. Between measurements, the P-Channel MOSFET (IRF9540) gate is open, and the device draws no current. During the two second heat pulse, the heater wire drew 0.55 and 1.12 A at 6 and 12 V, respectively. By decreasing the applied voltage from 12 to 6 V, the corresponding power draw per heat pulse decreased from 13.44 to 3.30 W, resulting in a 24.6% increase in battery life. With eight 1.2 V 2000 mAh AA batteries, the system operated for 14 days if measurements are made every 30 minutes. The nominal power draw outside of the heat pulse was 0.2 W during the 105 s of temperature monitoring and 0 W outside of the measurement period. Actual field operation times varied between a low of 11 and a high of 21

565   days depending on the outside temperature, as well as the brand and rating of NiMH battery

566   used. Longest operation times were obtained using 2300 mAh Energizer batteries.

567

568   *7.3. Laboratory Assessment of Sap Flow Measurement Accuracy*

569   With the DMA applied, sap flow estimated by the device closely matched that measured

570   gravimetrically (Figure 24). The relative error between device measurements and gravimetric

571   measurements was 10.6% when aggregating across both species (Table 1) with a slight

572   consistent underprediction in the device measurements. This underprediction is consistent with

573   other studies and is often attributed to imperfect estimation of wounding effects [36]. Prediction

574   accuracy was higher for *T. canadensis* than *A. saccharum* across all methods. The mean

575   gravimetric flow rates for *T. canadensis* and *A. saccharum* were 829.0 and 1602 g hr^{-1},

576   respectively. The lower flow rates in *T. canadensis* were reflected in the DMA algorithm; of the

577   63 independent measurements of sap flow in *T. canadensis*, 53 were identified as HRM (84%),

578   compared to 25 of 57 in *A. saccharum* (44%). All ten Tmax measurements associated with *T.*

579   *canadensis* occurred in one branch, which resulted in a lower mean absolute error and relative

580   percent error than any other method in either species due to the repeated measurements at the

581   same flow rate.
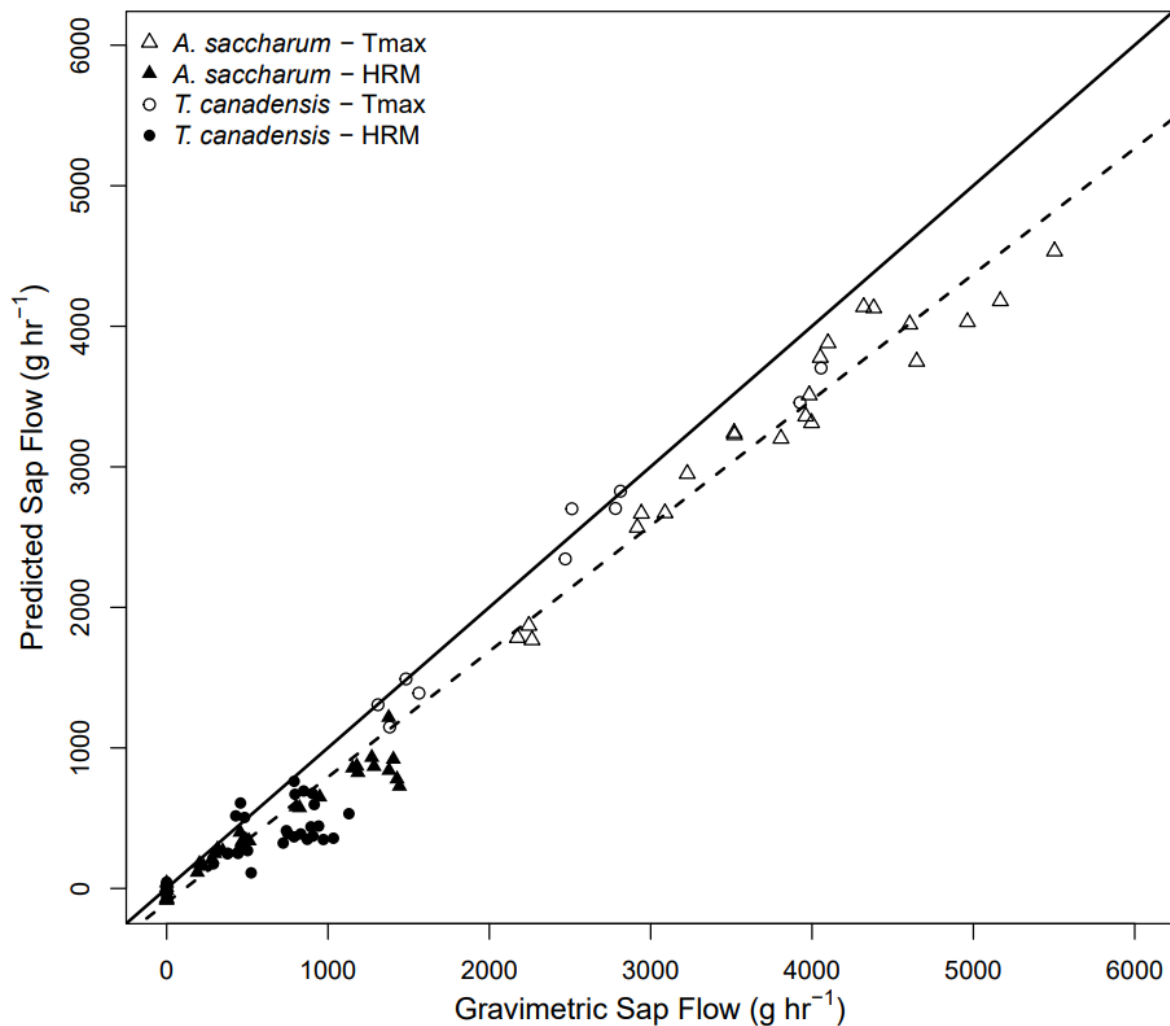
Figure 24: Correlation between the predicted sap flow measured via the HRM (solid) and Tmax (hollow) methods versus the gravimetric flow rate through branches of *A. saccharum* (triangle) and *T. canadensis* (circle). The solid line represents a 1 to 1 relationship and the dashed line represents the linear regression between the predicted and gravimetric sap flow using three (0.5, 1.5 and 2.5 cm) radial measurement points.

582

583
584
585
586
587

588

589

590

591

592

593

594

595

Table 1: Accuracy of each method in predicting gravimetric sap flow (g hr^{-1}). Error is the percent deviation from the slope derived from the linear regression between each method and the associated gravimetric sap flow. MAE is the mean absolute error and the maximum and minumum sap flow ranges for each method are measured in sap flow (F; g hr^{-1}).

Method	Error (%)	adj R^2	MAE (g hr^{-1})	Maximum F (g hr^{-1})	Minimum F (g hr^{-1})
Gravimetric				5503	0
HRM	36.6	0.71	199.8	1217	0
A. saccharum	55.8	0.70	193.1	1217	0
T. canadensis	19.8	0.71	205.2	762.4	0
Tmax	15.1	0.93	437.2	4534	649.4
A. saccharum	13.4	0.93	491.9	4534	649.4
T. canadensis	9.7	0.96	164.6	3703	1149
DMA	10.6	0.96	292.6	4534	0
A. saccharum	12.8	0.96	345.7	4534	0
T. canadensis	6.0	0.95	197.5	3703	0

The motivation for using the DMA is clear when evaluating the suitability of HRM and Tmax methods applied separately. The HRM method had a maximum sap flow measurement of 1200 g hr^{-1} and was not able to resolve medium or high flow rates (Table 1). In contrast, the Tmax method was unable to resolve low flow conditions with the minimum flow measurement around 494 g hr^{-1}. Besides limitations in range, the HR method had a 36.6% error and the Tmax method had a 15.1% error. While the percent error was higher for the HR method than the Tmax method, the overall magnitude of sap flow was lower which resulted in a lower overall MAE for the HR method. In a meta-analysis of every peer-reviewed published paper where the heat pulse velocity method was compared to independent measurements of plant water use, the mean R^2 values for the HR, Tmax and Dual methods were 0.916, 0.859 and 0.892, respectively, which are comparable with or exceeded by the values of 0.71, 0.93, and 0.96, found in this study when applying the DMA [36].

7.4. Field Deployment

The operating periods of the 12 field-installed devices over the field season are shown in Figure 25. On average, devices were operational 68% of the field season. Small data gaps generally occurred due to depletion of batteries and could be eliminated by more consistent replacement of batteries. Larger gaps typically reflect SD card malfunction, as seen in HH-MAP-9, HH-MAP-8,

619 and HH-HEM-2. In some cases, data corruption was not identified for several weeks while the

620 system otherwised appeared to be functioning properly, resulting in the very long gaps associated

621 with HH-MAP-7 and HH-HEM-9. Additionally, if SD card malfunction was identifed after Sept.

622 15 (Julian Day 258), the device was removed for the rest of the year, as seen in HH-MAP-7, HH-

623 HEM-4, and HH-HEM-9. In one case, HH-MAP-5, user error resulted in destruction of the

624 device (i.e., battery pack connected to wrong wires), which was then decommisioned for the

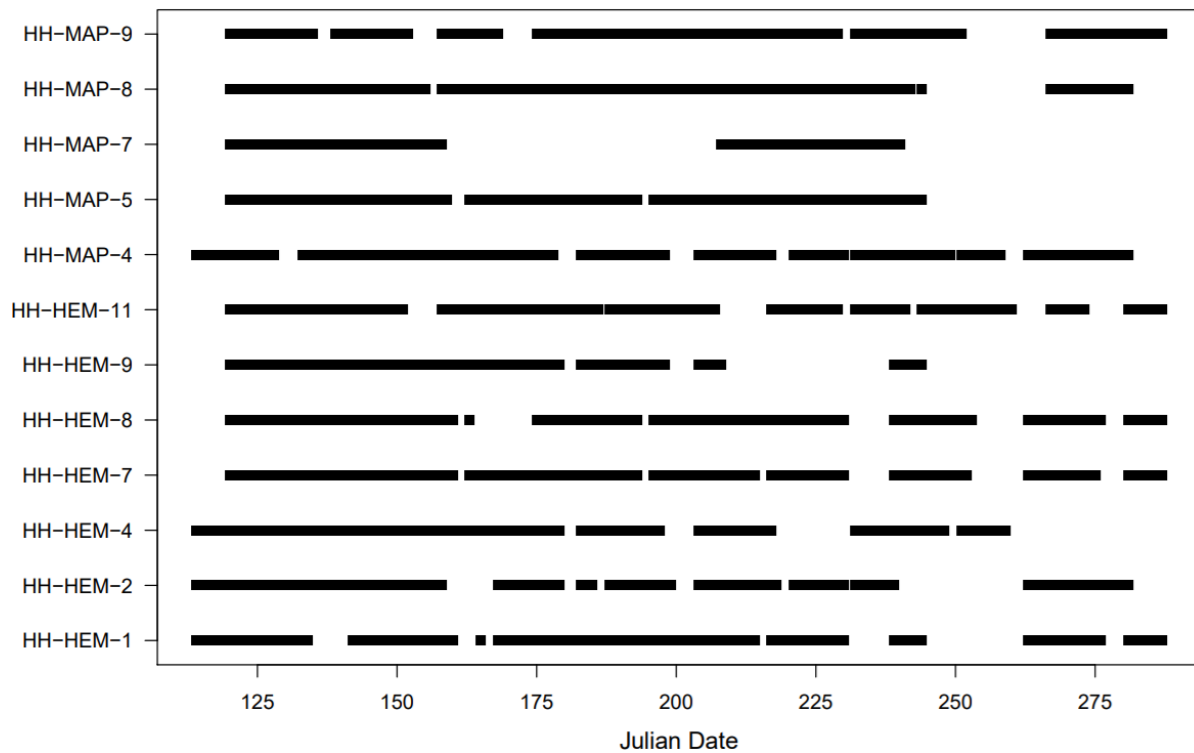625 remainder of the deployment period.

626

628 **Figure 25:** Time series demonstating the operations of 12 deployed custom sap flow sensors.

629

630   Outside of user error, the issues resulting in data gaps have been resolved. The SD card

631 malfuntion was identified as both a software and hardware issue; the software was adjusted to

632 more effectively write to the SD cards and SD cards specifically designed to operate in outdoor

633 environments were installed. More frequent field visits have eliminated the small gaps in data

634 due to battery depletion.

635   For two trees, sap flow measurements from the field deployment were compared with

636   vapor pressure deficit (VPD) measurements and seasonal phenological variations in order to

637   assess whether sap flow measurements were physically consistent with expected controls. VPD

638   is often presumed to be a dominant control on transpiration and correlation with VPD is

639   indicative of reasonable operation of the sap flow probes.

640   The relation of VPD with estimated sap flow displayed seasonal changes consistent with

641   phenological changes in the trees. Within the growing and dormant seasons, estimated sap flow

642   strongly correlated to VPD (Figure 26).
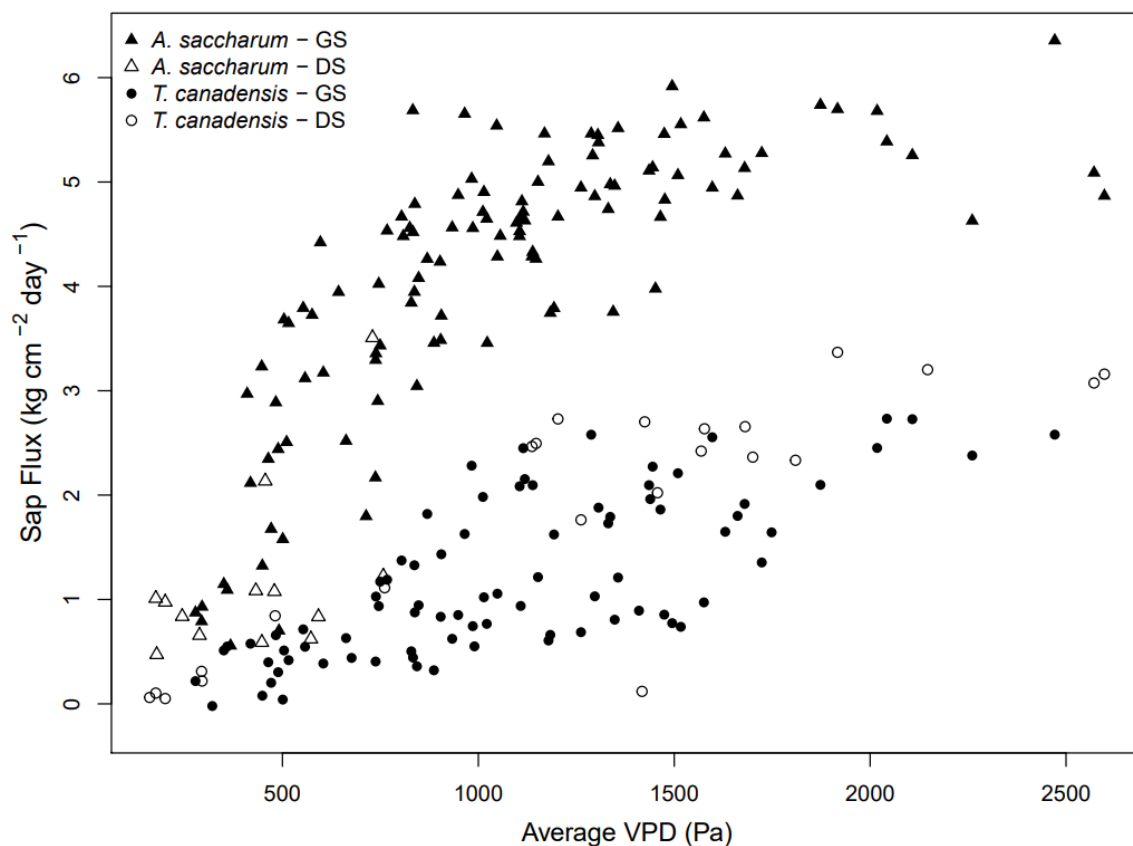

643

Figure 26: Correlation between daily sap flux and mean daily vapor pressure deficit (VPD)
between 8:00am and 4:00pm in in one individual of *A. saccharum* (triangle) and *T. canadensis*
(circle) (HH-MAP-4 and HH-HEM-4, respectively; see Figure 4). The data is classified by
measurements collected during the growing season (GS; between 5/20/2021 and 10/3/2021 for *A.
saccharum* and 6/1/2021 and 9/29/2021 for *T. canadensis*; solid), and during the dormant season
(DS; before 5/20/2021 and after 10/3/2021 for *A. saccharum* and before 6/1/2021 and after
9/29/2021 for *T. canadensis*; hollow).

651   The largest sap flow values for *T. canadensis* occurred prior to June 1. Before June 1, the

652   deciduous canopy was not fully developed and *T. canadensis* received maximum solar radiation

653   exposure and transpired at a high rate. After June 1, sap flow shifted down and remained lower

654   through the end of the season. In *A. saccharum* higher relative sap flow values occurred between

655   May 20 and October 3 when the canopy was developed and leaves were most active. When a

656   piecewise linear regression between daily VPD and daily estimated sap flow is calculated by

657   species and season, regression relationships are strong with an adjusted R^2 of 0.65 and 0.61, and

658   0.70 and 0.65, for *A. saccharum* and *T. canadensis* in the growing and dormant seasons,

659   respectively.

660   To further show the sensitivity of the sap flow device to subdaily changes as well as

661   seasonal changes, hourly sap flow for the beginning (Figure 27.a) and end (Figure 27.b) of the

662   growing season are presented for the deciduous species *A. saccharum.* Time periods correspond

663   to mid-May and early October. Sap flow increased progressively during the process of leaf out,

664   and slowly declined as leaves changed color and senesced. Negative sap flux values indicate

665   possible reverse flow scenarios. At the subdaily scale, there was an obvious diurnal variation in

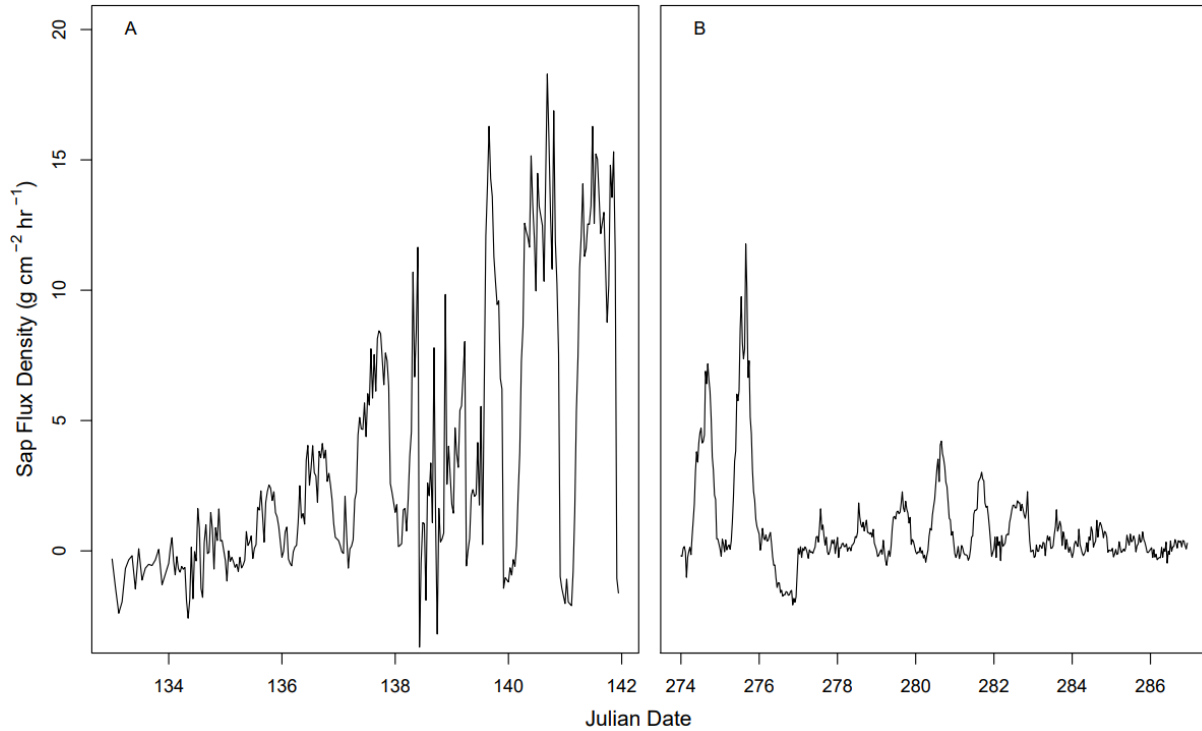666   sap flow with values approaching or subceeding zero during nighttime.

667

668

669

670

Figure 27: Time series of leaf out and senescense as measured by the J_s^5. Panels (A) and (B) depict the beginning and end of the growing season, respectively, in one individual of *A. saccharum* (HH-MAP-4; see Figure 24).

7.5. Potential Flexibility for Alternate Field Installations

By using rechargeable AA Ni-MH batteries, the J_s^5 can be self-contained within a small housing unit, allowing for simple and discrete deployment in the field. This device is ideal for urban site locations, where researchers may want equipment located higher up to avoid tampering, as well as remote site locations, where deploying and replacing large lead acid batteries may be prohibitive. In addition to the DMA detailed in this experiment, this device is capable of utilizing all HP methods, including the compensated heat pulse [33] and Sapflow+ [37] methods. Implementing the thermal dissipation method [38] is possible with modification to the probe design, however AA Ni-MH batteries are not suitable for this application.

 The battery lifespan of the J_s^5 can be further increased through a variety of methods. Taking advantage of the functionality of the microcontroller, this device can be programmed to measure SFD at different time intervals (e.g., every hour or every half hour), skip certain hours (e.g., nighttime hours), or limit the length of the subsequent temperature measurements. The HP

37

689   method requires only 5-10 s of background temperature measurements before the pulse is

690   applied, and subsequent temperature measurements range from 100-400 seconds, depending on

691   the HP method selected [29,32,33]. During field experiements, sampling every half hour, with

692   the exception of 20:00-01:00 and 02:00-05:00, and measuring temperature for 100 seconds

693   following the heat pulse, the J_s^5 was able to operate for 14 days before depleting the battery. This

694   battery life could be increased further still by using a lead acid battery. Based on the device's

695   power consumption through Ni-MH battery tests, we could expect a lifespan of up to 100 days

696   using a 12 V 18 Ahr lead acid battery under the standard sampling plan laid out in the

697   methodologies. This would allow for multiple devices to be operated for long periods of time

698   without the need to replace the batteries, as well as the inclusion of solar powered system for

699   indefinite sampling.

700

8. Conclusion

702   We developed a new device for measuring tree sap flow that provides a ten-fold cost savings

703   when compared to conventional commercial probes and dataloggers, as well as a 25% increase in

704   battery life, without sacrificing accuracy. Including the cost of the rechargeable Ni-MH batteries,

705   the J_s^5 costs < $150 when parts are bought in bulk. This offers an inexpensive, customizable,

706   reliable, and easy to construct SFD measuring device that expands the types of possible

707   experiments that could be implemented, including stand-scale transpiration estimates at the

708   resolution of individual trees [39] and radial sap flux analyses [40]. When compared to a meta-

709   data analysis of sap flow versus independent plant water use measurements, the J_s^5 performed

710   comporably or exceeded the mean R^2 values [36]. While the device functioned well, and

711   predicted gravimetric sap flow accurately (adjusted $R^2 = 0.96$, 10.6% error), improving the

712   collection of physiological parameters, the alignment of probes during instrumentation, and

713   quality of specific device components (such as SD cards) would lead to more accurate and

714   consistent SFD measurements.

715

Human and animal rights

717   No human or animal studies were conducted in this work.

718

719

723

724 **Literature Cited**

725 [1]   K.B. Wilson, P.J. Hanson, P.J. Mulholland, D.D. Baldocchi, S.D. Wullschleger, A
726   comparison of methods for determining forest evapotranspiration and its components: sap-
727   flow, soil water budget, eddy covariance and catchment water balance, Agric. For.
728   Meteorol. 106 (2001) 153–168. https://doi.org/10.1016/S0168-1923(00)00199-4.
729 [2]   S. Jasechko, Z.D. Sharp, J.J. Gibson, S.J. Birks, Y. Yi, P.J. Fawcett, Terrestrial water fluxes
730   dominated by transpiration, Nature. 496 (2013) 347–350.
731   https://doi.org/10.1038/nature11983.
732 [3]   W.H. Schlesinger, S. Jasechko, Transpiration in the global water cycle, Agric. For.
733   Meteorol. 189–190 (2014) 115–117. https://doi.org/10.1016/j.agrformet.2014.01.011.
734 [4]   S.L. Steinberg, M.J. McFarland, J.W. Worthington, Comparison of Trunk and Branch Sap
735   Flow with Canopy Transpiration in Pecan, J. Exp. Bot. 41 (1990) 653–659.
736 [5]   D.A. Devitt, M. Berkowitz, P.J. Schulte, R.L. Morris, Estimating Transpiration for Three
737   Woody Ornamental Tree Species using Stem-flow Gauges and Lysimetry, HortScience. 28
738   (1993) 320–322. https://doi.org/10.21273/HORTSCI.28.4.320.
739 [6]   D.G. Williams, W. Cable, K. Hultine, J.C.B. Hoedjes, E.A. Yepez, V. Simonneaux, S. Er-
740   Raki, G. Boulet, H.A.R. de Bruin, A. Chehbouni, O.K. Hartogensis, F. Timouk,
741   Evapotranspiration components determined by stable isotope, sap flow and eddy covariance
742   techniques, Agric. For. Meteorol. 125 (2004) 241–258.
743   https://doi.org/10.1016/j.agrformet.2004.04.008.
744 [7]   W.A. Dugas, J.S. Wallace, S.J. Allen, J.M. Roberts, Heat balance, porometer, and
745   deuterium estimates of transpiration from potted trees, Agric. For. Meteorol. 64 (1993) 47–
746   62. https://doi.org/10.1016/0168-1923(93)90093-W.
747 [8]   C. Poblete-Echeverría, S. Ortega-Farias, M. Zuñiga, S. Fuentes, Evaluation of compensated
748   heat-pulse velocity method to determine vine transpiration using combined measurements
749   of eddy covariance system and microlysimeters, Agric. Water Manag. 109 (2012) 11–19.
750   https://doi.org/10.1016/j.agwat.2012.01.019.
751 [9]   M. Lundblad, A. Lindroth, Stand transpiration and sapflow density in relation to weather,
752   soil moisture and stand characteristics, Basic Appl. Ecol. 3 (2002) 229–243.
753   https://doi.org/10.1078/1439-1791-00099.
754 [10] S.D. Wullschleger, P.J. Hanson, Sensitivity of canopy transpiration to altered precipitation
755   in an upland oak forest: evidence from a long-term field manipulation study, Glob. Change
756   Biol. 12 (2006) 97–109. https://doi.org/10.1111/j.1365-2486.2005.001082.x.
757 [11] D.S. Mackay, B.E. Ewers, M.M. Loranty, E.L. Kruger, On the representativeness of plot
758   size and location for scaling transpiration from trees to a stand, J. Geophys. Res.
759   Biogeosciences. 115 (2010). https://doi.org/10.1029/2009JG001092.
760 [12] G.W. Moore, J.A. Jones, B.J. Bond, How soil moisture mediates the influence of
761   transpiration on streamflow at hourly to interannual scales in a forested catchment, Hydrol.
762   Process. 25 (2011) 3701–3710. https://doi.org/10.1002/hyp.8095.

763 [13] R. Zimmermann, E.-D. Schulze, C. Wirth, E.-E. Schulze, K.C. Mcdonald, N.N.
764   Vygodskaya, W. Ziegler, Canopy transpiration in a chronosequence of Central Siberian
765   pine forests, Glob. Change Biol. 6 (2000) 25–37. https://doi.org/10.1046/j.1365-
766   2486.2000.00289.x.
767 [14] J.E. Drake, S.C. Davis, L.M. Raetz, E.H. DeLUCIA, Mechanisms of age-related changes in
768   forest production: the influence of physiological and successional changes, Glob. Change
769   Biol. 17 (2011) 1522–1535. https://doi.org/10.1111/j.1365-2486.2010.02342.x.
770 [15] M. Baret, S. Pepin, D. Pothier, Hydraulic limitations in dominant trees as a contributing
771   mechanism to the age-related growth decline of boreal forest stands, For. Ecol. Manag. 427
772   (2018) 135–142. https://doi.org/10.1016/j.foreco.2018.05.043.
773 [16] G.L. Miner, J.M. Ham, G.J. Kluitenberg, A heat-pulse method for measuring sap flow in
774   corn and sunflower using 3D-printed sensor bodies and low-cost electronics, Agric. For.
775   Meteorol. 246 (2017) 86–97. https://doi.org/10.1016/j.agrformet.2017.06.012.
776 [17] M.F. Cárdenas, C.L. Ramírez, J.D. Mejía, J.F. Escobar, Design and implementation of a
777   low-cost device for measuring sap flow in woody species, DYNA. 86 (2019) 214–220.
778   https://doi.org/10.15446/dyna.v86n208.72039.
779 [18] T.S. Jones, J.B. Winbourne, L.R. Hutyra, Ribbonized sap flow: an emerging technology for
780   the integration of sap flow sensor components onto a single platform, Ecosphere. 11 (2020)
781   e03135. https://doi.org/10.1002/ecs2.3135.
782 [19] J.G. Mickley, T.E. Moore, C.D. Schlichting, A. DeRobertis, E.N. Pfisterer, R. Bagchi,
783   Measuring microenvironments for global change: DIY environmental microcontroller units
784   (EMUs), Methods Ecol. Evol. 10 (2019) 578–584. https://doi.org/10.1111/2041-
785   210X.13128.
786 [20] Arduino IDE, Arduino.cc, 2021.
787 [21] L. Dalsgaard, Above and below Ground Gaps: The Effects of a Small Canopy Opening on
788   Throughfall, Soil Moisture and Tree Transpiration in Suserup Skov, Denmark, Ecol. Bull.
789   (2007) 81–102.
790 [22] P. Tor-ngern, R. Oren, A.C. Oishi, J.M. Uebelherr, S. Palmroth, L. Tarvainen, M. Ottosson-
791   Löfvenius, S. Linder, J.-C. Domec, T. Näsholm, Ecophysiological variation of transpiration
792   of pine forests: synthesis of new and published results, Ecol. Appl. 27 (2017) 118–133.
793   https://doi.org/10.1002/eap.1423.
794 [23] J.E. Fernández, P.J. Durán, M.J. Palomo, A. Diaz-Espejo, V. Chamorro, I.F. Girón,
795   Calibration of sap flow estimated by the compensation heat pulse method in olive, plum
796   and orange trees: relationships with xylem anatomy, Tree Physiol. 26 (2006) 719–728.
797   https://doi.org/10.1093/treephys/26.6.719.
798 [24] C.R. Ford, M.A. McGuire, R.J. Mitchell, R.O. Teskey, Assessing variation in the radial
799   profile of sap flux density in Pinus species and its effect on daily water use, Tree Physiol.
800   24 (2004) 241–249. https://doi.org/10.1093/treephys/24.3.241.
801 [25] R. Ren, G. Liu, M. Wen, R. Horton, B. Li, B. Si, The effects of probe misalignment on sap
802   flux density measurements and in situ probe spacing correction methods, Agric. For.
803   Meteorol. 232 (2017) 176–185. https://doi.org/10.1016/j.agrformet.2016.08.009.
804 [26] M.A. Forster, The importance of conduction versus convection in heat pulse sap flow
805   methods, Tree Physiol. 40 (2020) 683–694. https://doi.org/10.1093/treephys/tpaa009.
806 [27] M.W. Vandegehuchte, K. Steppe, Sap-flux density measurement methods: working
807   principles and applicability, Funct. Plant Biol. 40 (2013) 213.
808   https://doi.org/10.1071/FP12233.

809   [28] M.A. Forster, The Dual Method Approach (DMA) Resolves Measurement Range
810   Limitations of Heat Pulse Velocity Sap Flow Sensors, Forests. 10 (2019) 46.
811   https://doi.org/10.3390/f10010046.
812   [29] S.S.O. Burgess, M.A. Adams, N.C. Turner, C.R. Beverly, C.K. Ong, A.A.H. Khan, T.M.
813   Bleby, An improved heat pulse method to measure low and reverse rates of sap flow in
814   woody plants, Tree Physiol. 21 (2001) 589–598. https://doi.org/10.1093/treephys/21.9.589.
815   [30] G.J. Kluitenberg, T.E. Ochsner, R. Horton, Improved Analysis of Heat Pulse Signals for
816   Soil Water Flux Determination, Soil Sci. Soc. Am. J. 71 (2007) 53–55.
817   https://doi.org/10.2136/sssaj2006.0073N.
818   [31] Y. Cohen, M. Fuchs, G.C. Green, Improvement of the heat pulse method for determining
819   sap flow in trees, Plant Cell Environ. 4 (1981) 391–397. https://doi.org/10.1111/j.1365-
820   3040.1981.tb02117.x.
821   [32] G.J. Kluitenberg, J.M. Ham, Improved theory for calculating sap flow with the heat pulse
822   method, Agric. For. Meteorol. 126 (2004) 169–173.
823   https://doi.org/10.1016/j.agrformet.2004.05.008.
824   [33] R.H. Swanson, D.W.A. Whitfield, A Numerical Analysis of Heat Pulse Velocity Theory
825   and Practice, J. Exp. Bot. 32 (1981) 221–239.
826   [34] D.C. Marshall, Measurement of Sap Flow in Conifers by Heat Transport., Plant Physiol. 33
827   (1958) 385–396. https://doi.org/10.1104/pp.33.6.385.
828   [35] K. Steppe, D.J.W. De Pauw, T.M. Doody, R.O. Teskey, A comparison of sap flux density
829   using thermal dissipation, heat pulse velocity and heat field deformation methods, Agric.
830   For. Meteorol. 150 (2010) 1046–1056. https://doi.org/10.1016/j.agrformet.2010.04.004.
831   [36] M.A. Forster, How Reliable Are Heat Pulse Velocity Methods for Estimating Tree
832   Transpiration?, Forests. 8 (2017) 350. https://doi.org/10.3390/f8090350.
833   [37] M.W. Vandegehuchte, K. Steppe, Sapflow+: a four-needle heat-pulse sap flow sensor
834   enabling nonempirical sap flux density and water content measurements, New Phytol. 196
835   (2012) 306–317. https://doi.org/10.1111/j.1469-8137.2012.04237.x.
836   [38] A. Granier, A new method of sap flow measurement in tree stems, Ann. For. Sci. 45 (1985)
837   193–200.
838   [39] T. Kume, K. Otsuki, S. Du, N. Yamanaka, Y.-L. Wang, G.-B. Liu, Spatial variation in sap
839   flow velocity in semiarid region trees: its impact on stand-scale transpiration estimates,
840   Hydrol. Process. 26 (2012) 1161–1168. https://doi.org/10.1002/hyp.8205.
841   [40] A.B. Berdanier, C.F. Miniat, J.S. Clark, Predictive models for radial sap flux variation in
842   coniferous, diffuse-porous and ring-porous temperate trees, Tree Physiol. 36 (2016) 932–
843   941. https://doi.org/10.1093/treephys/tpw027.
844